AIMS Mathematics, 11(8): 26897–26926.
DOI: 10.3934/math.20261079
Received: 16 June 2026
Revised: 28 July 2026
Accepted: 12 August 2026
Published: 26 August 2026

https://www.aimspress.com/journal/Math

Research article

Adaptive power expansion iterative scheme for time-fractional Hindmarsh–Rose systems: Analysis of nonlinear signal propagation and memory dynamics

Othman Abdullah Almatroud*, Faten H. Damag, Sahar Albosaily and Marwa Ennaceur

Department of Mathematics, Faculty of Science, University of Ha'il, Ha'il 55473, Saudi Arabia

* **Correspondence:** Email: o.almatroud@uoh.edu.sa.

Abstract: This work developed an adaptive power expansion iterative scheme (APEIS) for numerically investigating nonlinear fractional systems involving Atangana–Baleanu–Caputo (ABC) operators. The proposed framework was applied to a time-fractional Hindmarsh–Rose (TF-HR) reaction–diffusion system to analyze memory-dependent signal propagation dynamics. Existence, uniqueness, convergence, and Hyers–Ulam stability results were established to provide the theoretical foundation of the proposed methodology. Numerical simulations were carried out for different fractional orders through approximate solution profiles, residual-error analysis, and wave-propagation investigations. A comparative study with the classical Adomian decomposition method (ADM) demonstrated close agreement between the two approaches, while APEIS consistently produced smaller residual errors and improved convergence behavior. The numerical results revealed that fractional memory effects strongly influence oscillatory dynamics and signal propagation. In particular, smaller fractional orders lead to smoother wave evolution with stronger memory effects, whereas larger fractional orders generate faster oscillatory behavior with weaker memory influence. These findings confirm the accuracy, efficiency, and reliability of the proposed APEIS framework for memory-dependent nonlinear reaction–diffusion systems.

Keywords: APEIS; ABC fractional derivative; TF-HR reaction–diffusion system; nonlinear signal propagation; wave propagation dynamics; residual error analysis; Hyers–Ulam stability
Mathematics Subject Classification: 34A08, 35R11, 35K57, 65M70, 65J15, 94A12

1. Introduction

Fractional calculus generalizes the classical concepts of differentiation and integration by extending them to arbitrary non-integer orders. Unlike local integer-order operators, fractional operators naturally incorporate memory and hereditary characteristics, making them suitable for describing systems whose

current behavior depends not only on the present state but also on past histories. The origins of fractional calculus date back to correspondence between Leibniz and L'Hopital in 1695, where the possibility of a derivative of order $\frac{1}{2}$ was first discussed. Subsequently, contributions of Riemann, Liouville, and Grunwald established the theoretical foundations that transformed these early ideas into a systematic mathematical framework [1, 2].

Over recent decades, numerous fractional operators have been introduced, including the Caputo–Fabrizio, Hilfer, Katugampola, and ABC derivatives, each characterized by different memory kernels and nonlocal structures. Compared with classical integer-order formulations, fractional models provide a more realistic description of memory-dependent phenomena and hereditary processes frequently encountered in practical systems [3]. Depending on the selected operator, the corresponding kernels may exhibit power-law, exponential, or Mittag–Leffler behavior, leading to different memory mechanisms, and dynamic responses. Consequently, fractional calculus has become an essential mathematical tool for both theoretical analysis and numerical modeling [4]. Recently, Zaidi [5] investigated the existence and stability properties of three-dimensional ABC fractional systems in locally compact Hausdorff spaces with applications to chaotic and fluid dynamics, while Zaidi [6] proposed a semi-analytical methodology for fractional dynamical systems with applications to wave propagation.

Fractional operators have found widespread applications in viscoelasticity, anomalous diffusion, heat transfer, control systems, electrochemistry, signal and image processing, bioengineering, and finance, where delayed responses and nonlocal interactions play essential roles [7, 8]. In many such applications, fractional models provide more accurate descriptions of experimental observations compared with classical approaches. As a consequence, research involving fractional theory, computational methods, and practical applications has expanded significantly. Partial differential equations (PDEs) remain fundamental tools for modeling transport phenomena, diffusion processes, and wave propagation. Nevertheless, classical PDEs often become inadequate when long-memory behavior or multi-scale interactions are involved. To overcome these limitations, fractional partial differential equations (FPDEs) have emerged as natural generalizations of integer-order models [9]. These equations have been successfully applied to anomalous transport processes, viscoelastic flows, turbulence, quantum mechanics, stochastic systems, geophysics, biological modeling, and financial mathematics [10, 11].

Due to the complexity associated with nonlinear fractional models, numerous analytical, and numerical techniques have been developed for constructing approximate solutions. These include transform-based approaches, decomposition methods, homotopy procedures, variational techniques, and numerical discretization schemes. Representative examples include SG expansions [12], algebraic methods [13], the fractional Newton method (FNM) [14], Laplace-transform approaches [2], variational iteration techniques [15], Sumudu decomposition methods [16], Adomian decomposition procedures [17], kernel Hilbert space techniques [18], scaling approaches [19], and the q-HATM framework [20]. These developments reflect the continuous effort toward constructing computational frameworks capable of simultaneously improving approximation accuracy, stability, and computational efficiency. Recently, Nikan et al. [21] proposed an improved local radial basis function method for the numerical solution of the time-fractional Black–Scholes model. Li et al. [22] investigated Turing instability and pattern formation in a diffusive predator–prey system with opportunistic predators and a weak effect, highlighting the rich dynamical behavior of nonlinear reaction–diffusion systems.

In this framework, we consider following general nonlinear fractional system:

$$\begin{cases} \mathcal{D}^{\sigma}_{0,\mu_m}\phi_k(\mu_i) = D_{\phi_k}\ \dfrac{\partial^n}{\partial\mu_1^n}\phi_k(\mu_i) + \phi_k^0\ \phi_k(\mu_i) + \mathcal{Q}_k\Big\{(\mu_i), \phi_k(\mu_i), \\ \phi_k(\mu_1, \mu_2, \cdots \mu_{m-1}, \mu_m - \xi), \phi_k\left[\mu_1, \mu_2, \cdots \mu_{m-1}, \mu_m - \mathcal{F}_k[(\phi_1\phi_2\cdots\phi_{s-1})(\mu_i)]\right]\Big\}, \\ \phi_k(\mu_i) = \varsigma_k(\mu_i),\ 0 \le \mu_m \le \rho_k, \\ \phi_k(\mu_1, \mu_2, \cdots, \mu_{m-1}, 0) = h_k(\mu_1, \mu_2, \cdots, \mu_{m-1}),\ k \in \{1, 2, \cdots, s\}, \end{cases} \tag{1.1}$$

for all

$$(\mu_i) = (\mu_1, \mu_2, \cdots, \mu_m) \in \Pi\Psi := \Psi \times [0, \mu_0]^{m-1},$$

where $\Psi \subset \mathbb{R}$, $\mu_0 > 0$, and $\mathcal{D}^{\sigma}_{0,\mu_m}$ denotes the ABC fractional derivative of order $0 < \sigma \le 1$. Moreover, $s, m, n \in \mathbb{N}$ and $\rho_k = \max\{\xi, \sup_t \mathcal{F}_k(t)\}$, subject to $\rho_k < \mu_0$ and $\xi > 0$ for all $k \in \{1, 2, \cdots, s\}$. The function $\mathcal{F}_k$ is assumed continuous on $(0, \rho_k]$, ς_k is bounded and continuous, $\mathcal{Q}_k$ is continuous and ϕ_k^0 are constant coefficients. As a practical application related to nonlinear signal propagation, consider the special case where $\alpha = 1$, $k = 3$, and $s = m = 2$, with $\mathcal{Q}_1 = \phi_2 - a_1\phi_1^3 + a_2\phi_1^2 - \phi_3 + I$, $\mathcal{Q}_2 = b_1 - b_2\phi_1^2$, $\mathcal{Q}_3 = c_1c_2(\phi_1 - c_3)$, $\phi_1^0 = 0$, $\phi_2^0 = -1$, and $\phi_3^0 = -c_1$. In this context, system (1.1) becomes classical HR reaction–diffusion oscillator system [23], which is one of most widely studied nonlinear oscillator models for investigating complex dynamical behaviors and nonlinear signal propagation mechanisms in modern signal environments. Here, μ_1 and μ_2 represent the spatial and temporal variables, respectively. The function ϕ_1 denotes the principal nonlinear oscillatory signal propagating through the signal dynamics, ϕ_2 represents the fast recovery variable responsible for rapid dynamic adjustments, and ϕ_3 represents the slow adaptation variable controlling long-term memory effects and delayed responses. The parameters $D_{\phi_1}, D_{\phi_2}, D_{\phi_3}$ are diffusion coefficients describing spatial propagation of information signals. For the constants: a_1 controls nonlinear damping, a_2 controls nonlinear excitation, b_1 represents recovery input, b_2 controls fast recovery coupling, c_1 determines the slow adaptation rate, c_2 controls slow adaptation coupling, c_3 denotes the activation threshold, and I represents the external input intensity.

Several studies have investigated fractional HR systems and their fractional extensions. Fateev and Polezhaev [23] studied interacting neuronal chains with nonlocal coupling governed by fractional and variable-order Laplace operators together with HR nonlinearities. Xue and Fu [24] examined fractional stochastic HR equations with memristive effects and established random attractors for long-term stochastic dynamics. Abro et al. [25] analyzed magnetized and demagnetized fractional HR neuron dynamics using fractal numerical simulations. Malik and Mir [26] developed a discrete multiplierless realization of the fractional-order HR model for efficient hardware and computational intelligence applications. Xiao [27] investigated stability and Hopf-type bifurcation phenomena in fractional-order HR neuronal systems.

Nonlinear signal systems frequently exhibit delayed responses, memory effects, and complex oscillatory interactions that classical integer-order models often fail to capture accurately. Fractional reaction–diffusion systems provide a natural framework for modeling such phenomena; however, obtaining reliable analytical solutions for nonlinear fractional models remains challenging. Furthermore, existing computational techniques may become difficult to implement when treating strongly nonlinear dynamical behaviors involving memory effects and adaptive responses. These challenges motivate the development of efficient analytical-numerical frameworks capable of

producing reliable approximations while preserving the physical interpretation of nonlinear wave dynamics.

Unlike existing analytical and semi-analytical methods, the proposed APEIS provides a unified framework that combines rigorous theoretical analysis with an adaptive iterative computational procedure. The proposed method establishes existence, uniqueness, convergence, and Hyers–Ulam stability within the same framework while generating accurate approximations for nonlinear fractional systems involving the ABC operator. Compared with the classical ADM, APEIS produces improved residual-error behavior and offers a more systematic treatment of memory-dependent nonlinear dynamics, making it an effective approach for the considered time-fractional Hindmarsh–Rose system.

Despite the significant progress achieved by existing analytical and numerical methods for nonlinear fractional systems, several challenges remain. Many available approaches mainly focus on the construction of approximate solutions without providing a unified theoretical framework that simultaneously establishes existence, uniqueness, convergence, and stability. Moreover, the numerical analysis of memory-dependent nonlinear signal propagation governed by the ABC fractional operator remains relatively limited. These limitations motivate the development of the proposed APEIS framework, which combines rigorous theoretical analysis with an efficient iterative computational procedure for nonlinear fractional systems.

The main contributions of this work are summarized as follows. A new APEIS is proposed for nonlinear fractional systems involving the ABC fractional operator. A unified theoretical framework is established through the analysis of existence, uniqueness, convergence, and Hyers–Ulam stability. The proposed framework is then applied to a time-fractional Hindmarsh–Rose reaction–diffusion system to investigate memory-dependent signal propagation. Finally, the effectiveness of the proposed method is validated through numerical simulations and comparisons with the classical Adomian decomposition method, demonstrating its accuracy, and reliability.

The remainder of the paper is organized as follows. Section 2 presents the mathematical preliminaries and fundamental definitions. Section 3 develops the APEIS framework and establishes its convergence and Hyers–Ulam stability properties. Section 4 applies the proposed methodology to the TF-HR reaction–diffusion system and derives the corresponding iterative approximations. Section 5 presents numerical investigations, including residual error analysis, convergence studies, a comparison with the classical ADM, and wave-propagation simulations for different fractional orders.

2. Preliminaries

Let ϕ be any map on $\Pi\Psi$. The ABC integral map of $\phi(\mu_i)$ with order $\sigma > 0$ is given by [28, 29]

$$\mathcal{I}^{\sigma}_{0,\mu_m}\phi(\mu_i) = \frac{1-\sigma}{K^{\sigma}}\ \phi(\mu_i) + \frac{\sigma}{\Gamma(\sigma)K^{\sigma}}\int_0^{\mu_m}(\mu_m-\varrho)^{\sigma-1}\phi(\mu_1,\mu_2,\cdots,\mu_{m-1},\varrho)d\varrho \tag{2.1}$$

for all $0 < \sigma < 1$. The ABC derivative map of $\phi(\mu_i)$ with order $\sigma > 0$ is

$$\mathcal{D}^{\sigma}_{0,\mu_m}\phi(\mu_i) = \frac{K^{\sigma}}{1-\sigma}\int_0^{\mu_m}E_{\sigma}\left(\frac{-\sigma(\mu_m-\varrho)^{\sigma}}{1-\sigma}\right)\frac{\partial^n}{\partial\varrho^n}\phi(\mu_1,\mu_2,\cdots,\mu_{m-1},\varrho)d\varrho \tag{2.2}$$

for all $n-1 < \sigma < n$ and $\mathcal{D}^{\sigma}_{0,\mu_m}\phi(\mu_i) = \dfrac{\partial^n}{\partial\mu_m^n}\phi(\mu_i)$ for all $\sigma := n \in \mathbb{N}$, where $E_{\sigma}(\cdot)$ denotes the Mittag-Leffler function and $K^{\cdot}$ is a normalization function satisfying $K^0 = K^1 = 1$.

For $\mu_m \geq 0$ and $n-1 < \sigma < n$, we have

$$\mathcal{D}^{\sigma}_{0,\mu_m}\mathcal{I}^{\sigma}_{0,\mu_m}\phi(\mu_i) = \phi(\mu_i), \tag{2.3}$$

$$\mathcal{D}^{\sigma}_{0,\mu_m}\mu_m^{\delta} = \frac{\Gamma(\delta+1)}{\Gamma(\delta+1-\sigma)}\mu_m^{\delta-\sigma}, \tag{2.4}$$

$$\mathcal{I}^{\sigma}_{0,\mu_m}\mathcal{D}^{\sigma}_{0,\mu_m}\phi(\mu_i) = \phi(\mu_i) - \sum_{k=0}^{n-1}\frac{\mu_m^k}{k!}\frac{\partial^k}{\partial\mu_m^k}\phi(\mu_i)\bigg|_{\mu_m=0}, \tag{2.5}$$

where $n \in \mathbb{N}$ and $\delta > -1$.

Let $\Psi \subset \mathbb{R}$ be compact and $\mathbb{R}^{\Pi\Psi}$ denote the set of all maps from $\Pi\Psi$ into $\mathbb{R}$. Define

$$C^n(\Pi\Psi, \mathbb{R}) = \{\phi : \Pi\Psi \to \mathbb{R} \mid D^{\alpha}\phi \text{ is continuous on } \Pi\Psi \text{ for all multi-indices } \alpha \text{ with } |\alpha| \leq n\},$$

where

$$|\alpha| = \alpha_1 + \cdots + \alpha_m, \quad D^{\alpha}\phi = \frac{\partial^{|\alpha|}\phi}{\partial\mu_1^{\alpha_1}\cdots\partial\mu_m^{\alpha_m}}$$

for all $\alpha = (\alpha_1, \ldots, \alpha_m) \in \mathbb{N}^m$. Since Ψ is a compact set in $\mathbb{R}$, it follows that $C^n(\Pi\Psi, \mathbb{R})$ is a Banach space equipped with the norm

$$\|\phi\|_{C^n} = \max_{|\alpha|\leq n}\sup_{(\mu_i)\in\Pi\Psi}|D^{\alpha}\phi(\mu_i)|.$$

Let $\mathcal{B} := \prod_{k=1}^{s} C_{\Pi\Psi_n}$ be a Banach space with the norm

$$\|(\phi_1, \phi_2, \cdots, \phi_s)\|_{\mathcal{B}} = \max\{\|\phi_k\|_{C^n} : k = 1, 2, \cdots, s\},$$

where $C_{\Pi\Psi_n} := C^n(\Pi\Psi, \mathbb{R}) \subseteq \mathbb{R}^{\Pi\Psi}$. Since $\Pi\Psi$ is a compact set in $\mathbb{R}^2$, then for all balls $R(\mu_0', \epsilon)$ in $\mathbb{R}$,

$$\{\curlyvee(Z, R(\mu_0', \epsilon)) : Z \text{ is compact set in } \Pi\Psi,\ \mu_0' \in \mathbb{R},\ \epsilon > 0\}$$

forms a subbase for the compact-open topology on $C_{\Pi\Psi_n}$, where

$$\curlyvee(Z, R(\mu_0', \epsilon)) = \{\phi_k \in C_{\Pi\Psi_n} : \phi_k(Z) \subset R(\mu_0', \epsilon)\}.$$

Since $\Pi\Psi \subset \mathbb{R}$ is compact, the compact-open topology on $C_{\Pi\Psi_n}$ is the same as the topology given by the norm

$$\|\phi\|_{\infty} = \sup_{(\mu_i)\in\Pi\Psi}|\phi(\mu_i)|.$$

So in this work, the space $\mathbb{R}^{\Pi\Psi}$ will be equipped with the compact-open topology. For every $k \in \{1, 2, \cdots, s\}$, define $\mathbb{G}_{\phi_k} : \Pi\Psi \times \prod_{j=1}^{s}\mathbb{R}^{\Pi\Psi} \to \mathbb{R}$ by

$$\mathbb{G}_{\phi_k}((\mu_i), (\phi_j)) = D_{\phi_k}\frac{\partial^n}{\partial\mu_1^n}\phi_k(\mu_i) + \phi_k^0\ \phi_k(\mu_i) + \mathcal{Q}_k\Big\{(\mu_i), \phi_k(\mu_i),$$
$$\phi_k(\mu_1, \mu_2, \cdots\mu_{m-1}, \mu_m - \xi), \phi_k\left[\mu_1, \mu_2, \cdots\mu_{m-1}, \mu_m - \mathcal{F}_k[(\phi_1\phi_2\cdots\phi_{s-1})(\mu_i)]\right]\Big\}$$

for all $(\mu_i) \in \Pi\Psi$ and $(\phi_j) := (\phi_1, \phi_2, \cdots, \phi_s) \in \prod_{j=1}^{s}\mathbb{R}^{\Pi\Psi}$. By the ABC integral map of (1.1) and by (2.5),

$$\phi_k(\mu_i) = h_k(\mu_1, \mu_2, \cdots, \mu_{m-1}) + \frac{1-\sigma}{K^{\sigma}}\mathbb{G}_{\phi_k}((\mu_i), (\phi_j))$$
$$+ \frac{\sigma}{\Gamma(\sigma)K^{\sigma}}\int_0^{\mu_m}(\mu_m - \varrho)^{\sigma-1}\ \mathbb{G}_{\phi_k}(\mu_1, \mu_2, \cdots, \mu_{m-1}, \varrho, (\phi_j))d\varrho.$$

For every $k \in \{1, 2, \cdots, s\}$, define the operator $\mathbb{A}_{\phi_k} : \prod_{j=1}^{s} \mathbb{R}^{\Pi\Psi} \to \mathbb{R}^{\Pi\Psi}$ by

$$\mathbb{A}_{\phi_k}(\phi_j)(\mu_i) = h_k(\mu_1, \mu_2, \cdots, \mu_{m-1}) + \frac{1-\sigma}{K^\sigma}\mathbb{G}_{\phi_k}((\mu_i), (\phi_j)) + \frac{\sigma}{\Gamma(\sigma)K^\sigma}\int_0^{\mu_m} (\mu_m - \varrho)^{\sigma-1}\ \mathbb{G}_{\phi_k}(\mu_1, \mu_2, \cdots, \mu_{m-1}, \varrho, (\phi_j))d\varrho$$

for all $(\mu_i) \in \Pi\Psi$ and $(\phi_j) \in \prod_{j=1}^{s} \mathbb{R}^{\Pi\Psi}$. If there is $\omega_{\phi_k} > 0$ such that

$$\left|\mathbb{G}_{\phi_k}((\mu_i), (\phi_j)) - \mathbb{G}_{\phi_k}((\mu_i'), (\phi_j'))\right| \leq \omega_{\phi_k} \left\|(\phi_j) - (\phi_j')\right\|_{\mathcal{B}}$$

for all $(\mu_i), (\mu_i') \in \Pi\Psi$ and $(\phi_j), (\phi_j') \in \prod_{j=1}^{s} \mathbb{R}^{\Pi\Psi}$, then $\mathbb{G}_{\phi_k}$ is said to have the Lipschitz property.

The following lemma establishes a basic property of the operator that will be used throughout the subsequent analysis.

Lemma 2.1. For every $k \in \{1, 2, \cdots, s\}$, if $\mathbb{G}_{\phi_k}$ satisfies a Lipschitz condition on $\Pi\Psi \times \prod_{j=1}^{s} \mathbb{R}^{\Pi\Psi}$, then $\mathbb{A}_{\phi_k}$ also satisfies a Lipschitz condition.

Proof. Let $k \in \{1, 2, \cdots, s\}$. Assume that there is $\omega_{\phi_k} > 0$ such that

$$\left|\mathbb{G}_{\phi_k}((\mu_i), (\phi_j)) - \mathbb{G}_{\phi_k}((\mu_i'), (\phi_j'))\right| \leq \omega_{\phi_k} \left\|(\phi_j) - (\phi_j')\right\|_{\mathcal{B}}$$

for all $(\mu_i), (\mu_i') \in \Pi\Psi$ and $(\phi_j), (\phi_j') \in \prod_{j=1}^{s} \mathbb{R}^{\Pi\Psi}$. Then for every $(\mu_i) \in \Pi\Psi$,

$$\begin{aligned}
&\left|\mathbb{A}_{\phi_k}(\phi_j)(\mu_i) - \mathbb{A}_{\phi_k}(\phi_j')(\mu_i)\right| \\
&\leq \frac{1-\sigma}{K^\sigma}\left|\mathbb{G}_{\phi_k}((\mu_i), (\phi_j)) - \mathbb{G}_{\phi_k}((\mu_i), (\phi_j'))\right| \\
&\quad + \frac{\sigma}{\Gamma(\sigma)K^\sigma}\left|\int_0^{\mu_m} (\mu_m - \varrho)^{\sigma-1}\Big(\mathbb{G}_{\phi_k}(\mu_1, \ldots, \mu_{m-1}, \varrho, (\phi_j)) - \mathbb{G}_{\phi_k}(\mu_1, \ldots, \mu_{m-1}, \varrho, (\phi_j'))\Big)d\varrho\right| \\
&\leq \left[\frac{(1-\sigma)\omega_{\phi_k}}{K^\sigma} + \frac{\mu_0^\sigma \omega_{\phi_k}}{\Gamma(\sigma)K^\sigma}\right]\left\|(\phi_j) - (\phi_j')\right\|_{\mathcal{B}}.
\end{aligned}$$

Therefore

$$\left\|\mathbb{A}_{\phi_k}(\phi_j) - \mathbb{A}_{\phi_k}(\phi_j')\right\| \leq \left[\frac{(1-\sigma)\omega_{\phi_k}}{K^\sigma} + \frac{\mu_0^\sigma \omega_{\phi_k}}{\Gamma(\sigma)K^\sigma}\right]\left\|(\phi_j) - (\phi_j')\right\|_{\mathcal{B}}. \tag{2.6}$$

Hence $\mathbb{A}_{\phi_k}$ satisfies a Lipschitz condition. □

For every $k \in \{1, 2, \cdots, s\}$, define $\mathcal{R}_{\phi_k} : \mathcal{B} \to \mathbb{R}^{\Pi\Psi}$ as

$$\begin{aligned}
\mathcal{R}_{\phi_k}(\phi_j) = D_{\phi_k}\ &\frac{\partial^n}{\partial\mu_1^n}\phi_k(\mu_i) + \phi_k^0\ \phi_k(\mu_i) + \mathcal{Q}_k[\pi_1, \pi_2, \cdots \pi_m, \phi_k, \phi_k \circ (\pi_1, \pi_2, \cdots \pi_{m-1} \times \zeta_\xi(\mu_m)), \\
&\phi_k \circ (\pi_1, \pi_2, \cdots \pi_{m-1} \times \zeta_\xi(\mathcal{F}_k \circ (\phi_1, \phi_2, \cdots, \phi_{s-1})))]
\end{aligned} \tag{2.7}$$

for all $(\phi_j) \in \mathcal{B}$, where $\zeta_\xi(x) = x - \xi$ and $\pi_{1,2,\cdots,m}$ are the usual projection maps. For the continuity of $\mathcal{R}_{\phi_k}$, we have that if $\mathbb{G}_{\phi_k}$ has a Lipschitz property, then

$$|\langle \mathcal{R}_{\phi_k}(\phi_j) - \mathcal{R}_{\phi_k}(\phi_j'), (\phi_j) - (\phi_j')\rangle| \leq \omega_{\phi_k} \left\|(\phi_j) - (\phi_j')\right\|_{\mathcal{B}}^2.$$

Assume that the following conditions hold:

D1: Consider $C_{\Pi\Psi_n}$ a space under the compact-open topology and $\phi_k \in C_{\Pi\Psi_n}$ for all $k \in \{1, 2, \cdots, s\}$ and Ψ is a compact set in $\mathbb{R}$.

D2: For every $k \in \{1, 2, \cdots, s\}$, $\exists\ \xi_{\phi_k} > 0$, where $\left|\mathbb{G}_{\phi_k}((\mu_i), (\phi_j))\right| \leq \xi_{\phi_k}$.

D3: For every $k \in \{1, 2, \cdots, s\}$, $\mathbb{G}_{\phi_k}$ has a Lipschitz property with constant $\omega_{\phi_k} > 0$.

The assumptions D1–D3 are standard sufficient conditions used to establish the existence, uniqueness, and convergence of the proposed iterative framework. Although they may be conservative for some nonlinear problems, they provide a rigorous theoretical foundation for the analysis developed in this work.

Using the previous lemma, we now establish the existence and uniqueness result for the proposed fractional system.

Theorem 2.2. Let D1–D3 be satisfied with

$$\left[\frac{1-\sigma}{K^\sigma} + \frac{\mu_0^\sigma}{\Gamma(\sigma)K^\sigma}\right]\sum_{k=1}^{s}\omega_{\phi_k} < 1. \tag{2.8}$$

Then (1.1) has a unique solution.

Proof. Define $\mathbb{A} : \mathcal{B} \to \mathcal{B}$ by

$$\mathbb{A}(\phi_j) = \left(\mathbb{A}_{\phi_1}(\phi_j), \mathbb{A}_{\phi_2}(\phi_j), \ldots, \mathbb{A}_{\phi_s}(\phi_j)\right).$$

By D3 and Lemma 2.1, for any $(\phi_j), (\phi'_j) \in \mathcal{B}$, we obtain

$$\|\mathbb{A}(\phi_j) - \mathbb{A}(\phi'_j)\|_{\mathcal{B}} \leq \left[\frac{1-\sigma}{K^\sigma} + \frac{\mu_0^\sigma}{\Gamma(\sigma)K^\sigma}\right]\left(\sum_{k=1}^{s}\omega_{\phi_k}\right)\|(\phi_j) - (\phi'_j)\|_{\mathcal{B}}.$$

Since

$$\left[\frac{1-\sigma}{K^\sigma} + \frac{\mu_0^\sigma}{\Gamma(\sigma)K^\sigma}\right]\sum_{k=1}^{s}\omega_{\phi_k} < 1,$$

then $\mathbb{A}$ satisfies the contraction property on the Banach space $\mathcal{B}$. Hence an application of the Banach contraction principle guarantees the existence of a unique fixed element of $\mathbb{A}$. $(\phi_j) \in \mathcal{B}$ such that $\mathbb{A}(\phi_j) = (\phi_j)$. Hence (1.1) has a unique solution. □

3. Construction and analysis of the APEIS

In this section, we develop the APEIS for constructing approximate solutions of the nonlinear fractional system introduced previously. Since Theorem 2.2 established the existence and uniqueness of solutions under suitable assumptions, this result provides the theoretical foundation required for the constructing reliable iterative approximations. The proposed APEIS is formulated by transforming fractional system into an equivalent integral representation and recursively generating adaptive power expansion terms. Furthermore, convergence and stability properties of the proposed procedure are investigated to demonstrate the reliability and effectiveness of the method for nonlinear fractional systems.

Lemma 3.1. Let $0 < \sigma < 1$. Then

$$\mathcal{D}^{\sigma}_{0,\mu}\,(\mu^{n\sigma}) = \frac{K^{\sigma}\Gamma(n\sigma+1)}{(1-\sigma)\Gamma(n\sigma-\sigma+1)}\,\mu^{n\sigma-\sigma}\;X_n(\mu), \tag{3.1}$$

where

$$X_n(\mu) := \sum_{m=0}^{\infty} \frac{(-1)^m \left(\frac{\sigma}{1-\sigma}\right)^m \mu^{m\sigma}}{\Gamma((n+m)\sigma+1)}. \tag{3.2}$$

Proof. Note that

$$\begin{aligned}
\mathcal{D}^{\sigma}_{0,\mu}\,(\mu^{n\sigma}) &= \frac{K^{\sigma}}{1-\sigma}\int_0^{\mu} E_{\sigma}\left(\frac{-\sigma(\mu-\lambda)^{\sigma}}{1-\sigma}\right)\frac{\partial}{\partial\lambda}(\lambda^{n\sigma})d\lambda \\
&= \frac{K^{\sigma}}{1-\sigma}\,n\sigma\int_0^{\mu} E_{\sigma}\left(\frac{-\sigma(\mu-\lambda)^{\sigma}}{1-\sigma}\right)\lambda^{n\sigma-1}d\lambda \\
&= \frac{K^{\sigma}}{1-\sigma}\,n\sigma\int_0^{\mu} \lambda^{n\sigma-1}\sum_{m=0}^{\infty}\frac{(-1)^m\left(\frac{\sigma}{1-\sigma}\right)^m(\mu-\lambda)^{m\sigma}}{\Gamma(m\sigma+1)}d\lambda \\
&= \frac{K^{\sigma}}{1-\sigma}\,n\sigma\sum_{m=0}^{\infty}\frac{(-1)^m\left(\frac{\sigma}{1-\sigma}\right)^m}{\Gamma(m\sigma+1)}\int_0^{\mu}(\mu-\lambda)^{m\sigma}\lambda^{n\sigma-1}d\lambda.
\end{aligned} \tag{3.3}$$

Note that

$$\int_0^{\mu}(\mu-\lambda)^{m\sigma}\lambda^{n\sigma-1}d\lambda = \mu^{n\sigma+m\sigma}\,\frac{\Gamma(n\sigma)\Gamma(m\sigma+1)}{\Gamma(n\sigma+m\sigma+1)}.$$

□

For every $k \in \{1, 2, \cdots, s\}$ in (1.1), consider a power series

$$\sum_{n=0}^{\infty} a_{k,n}(\mu_1, \mu_2, \ldots, \mu_{m-1})(\mu_m - a)^{n\sigma} = A_0 + A_1(\mu_m - a)^{\sigma} + A_2(\mu_m - a)^{2\sigma} + \cdots, \tag{3.4}$$

which is called a generalized fractional power series (GFPS) about a such that $a_{k,n}(\mu_1, \mu_2, \ldots, \mu_{m-1})$ are coefficients, where $0 < \sigma \leq 1$ and $\mu_m \geq a$.

The following lemma provides the coefficient representation of the generalized fractional power series used in the proposed method.

Lemma 3.2. For every $k \in \{1, 2, \cdots, s\}$, consider the GFPS notation of $\mathcal{T}^k$ about $a = 0$ of the form

$$\mathcal{T}^k(\mu_m) = \sum_{n=0}^{\infty} a_{k,n}(\mu_1, \mu_2, \ldots, \mu_{m-1})\mu_m^{n\sigma}, \tag{3.5}$$

where $0 < \sigma < 1$, $0 \leq \mu_m \leq \rho$, and $\rho = \max\{\rho_k : k \in \{1, 2, \cdots, s\}\}$. If $\mathcal{T}^k(\mu_m)$, $D^{n\sigma}_{0,\mu_m}\mathcal{T}^k(\mu_m) \in C[0, \rho]$ for all $k \in \{1, 2, \cdots, s\}$ and for all $n \in \mathbb{N}$, then $a_{k,n}(\mu_1, \mu_2, \ldots, \mu_{m-1})$ are given by

$$a_{k,n}(\mu_1, \mu_2, \ldots, \mu_{m-1}) = \frac{D^{n\sigma}_{0,\mu_m}\mathcal{T}^k(\mu_m)}{\Gamma(K^{\sigma}, \sigma, n)}\Big|_{\mu_m=0}, \tag{3.6}$$

where $D^{n\sigma}_{0,\mu_m} = D^{\sigma}_{0,\mu_m} \circ D^{\sigma}_{0,\mu_m} \circ \cdots \circ D^{\sigma}_{0,\mu_m}$ (n times), ρ is a convergence radius, and

$$\Gamma(K^{\sigma}, \sigma, n) := \frac{K^{\sigma}}{1-\sigma}\,\frac{\Gamma(n\sigma+1)}{\Gamma(2n\sigma-\sigma+1)\Gamma(1-n\sigma+\sigma)}\left(\frac{\sigma}{\sigma-1}\right)^{n-1}.$$

Proof. By Lemma 3.1,

$$
\begin{aligned}
D^{\sigma}_{0,\mu_m}\mathcal{T}^k(\mu_m) &= \sum_{n=1}^{\infty} a_{k,n}(\mu_1,\mu_2,\ldots,\mu_{m-1})\, D^{\sigma}_{0,\mu_m}(\mu_m^{n\sigma}) \\
&= \sum_{n=1}^{\infty} a_{k,n}(\mu_1,\mu_2,\ldots,\mu_{m-1})\,\frac{K^{\sigma}\Gamma(n\sigma+1)}{(1-\sigma)\Gamma(n\sigma-\sigma+1)}\,\mu_m^{n\sigma-\sigma}\; X_n(\mu_m) \\
&= \sum_{n=1}^{\infty} a_{k,n}(\mu_1,\mu_2,\ldots,\mu_{m-1})\,\frac{K^{\sigma}\Gamma(n\sigma+1)}{(1-\sigma)\Gamma(n\sigma-\sigma+1)}\,\mu_m^{n\sigma-\sigma}\;\sum_{q=0}^{\infty}\frac{(-1)^q\left(\frac{\sigma}{1-\sigma}\right)^q\mu_m^{q\sigma}}{\Gamma((n+q)\sigma+1)} \\
&= \sum_{n=1}^{\infty} a_{k,n}(\mu_1,\mu_2,\ldots,\mu_{m-1})\,\frac{K^{\sigma}\Gamma(n\sigma+1)}{(1-\sigma)\Gamma(n\sigma-\sigma+1)}\;\sum_{q=0}^{\infty}\frac{(-1)^q\left(\frac{\sigma}{1-\sigma}\right)^q}{\Gamma((n+q)\sigma+1)}\mu_m^{(n-1)\sigma+q\sigma}.
\end{aligned}
$$

Relabelling the index with $d = n-1$:

$$
D^{\sigma}_{0,\mu_m}\mathcal{T}^k(\mu_m) = \sum_{d=0}^{\infty} a_{k,d+1}(\mu_1,\mu_2,\ldots,\mu_{m-1})\frac{K^{\sigma}\Gamma((d+1)\sigma+1)}{(1-\sigma)\Gamma(d\sigma+1)}\;\sum_{q=0}^{\infty}\frac{(-1)^q\left(\frac{\sigma}{1-\sigma}\right)^q}{\Gamma((d+q+1)\sigma+1)}\mu_m^{d\sigma+q\sigma}.
$$

Setting $\mu_m = 0$ removes all terms with $d \geq 1$, since $\mu_m^{d\sigma+q\sigma} = 0$, so we get

$$
D^{\sigma}_{0,\mu_m}\mathcal{T}^k(\mu_m)\Big|_{\mu_m=0} = a_{k,1}(\mu_1,\mu_2,\ldots,\mu_{m-1})\,\frac{K^{\sigma}}{1-\sigma}.
$$

Define recursively $\mathcal{T}_0^k(\mu_m) = \mathcal{T}^k(\mu_m)$ and

$$
\mathcal{T}_d^k(\mu_m) = D^{\sigma}_{0,\mu_m}\mathcal{T}_{d-1}^k(\mu_m) = D^{k\sigma}_{0,\mu_m}\mathcal{T}^k(\mu_m).
$$

Using (2.2) repeatedly, by induction, we get

$$
\begin{aligned}
D^{k\sigma}_{0,\mu_m}\mathcal{T}^k(\mu_m) &= \mathcal{T}_d^k(\mu_m) \\
&= \sum_{k=n}^{\infty} a_{k,n}(\mu_1,\mu_2,\ldots,\mu_{m-1})\,\frac{K^{\sigma}\Gamma(n\sigma+1)}{(1-\sigma)\Gamma(n\sigma-d\sigma+1)}\,\mu_m^{n\sigma-k\sigma}\;\sum_{q=0}^{\infty}\frac{(-1)^q\left(\frac{\sigma}{1-\sigma}\right)^q\mu_m^{q\sigma}}{\Gamma((n+q)\sigma+1)}.
\end{aligned}
\tag{3.7}
$$

Set $d = n$ in (3.7) to get

$$
D^{n\sigma}_{0,\mu_m}\mathcal{T}^k(\mu_m)\Big|_{\mu_m=0} = a_{k,n}(\mu_1,\mu_2,\ldots,\mu_{m-1})\frac{K^{\sigma}}{1-\sigma}\frac{\Gamma(n\sigma+1)}{\Gamma(2n\sigma-\sigma+1)\Gamma(1-n\sigma+\sigma)}\left(\frac{\sigma}{\sigma-1}\right)^{n-1}.
$$

Hence

$$
a_{k,n}(\mu_1,\mu_2,\ldots,\mu_{m-1}) = \frac{D^{n\sigma}_{0,\mu_m}\mathcal{T}^k(\mu_m)}{\Gamma(K^{\sigma},\sigma,n)}\Big|_{\mu_m=0}.
$$

This completes the proof. □

In (1.1), for every $k \in \{1,2,\cdots,s\}$, consider a power series

$$
\phi_k(\mu_i) = \sum_{n=0}^{\infty}\mathcal{T}_n^k(\mu_1,\mu_2,\ldots,\mu_{m-1})\,\mu_m^{n\sigma},(\mu_i) \in \Pi\Psi,\ 0 \leq \mu_m \leq \rho. \tag{3.8}
$$

Based on the previous result, we now derive the general expansion formula for the proposed iterative approximation.

Theorem 3.3. If $D^{n\sigma}_{0,\mu_m}\phi_k(\mu_i), n = 0, 1, 2, 3, \ldots$, are continuous for all $k \in \{1, 2, \cdots, s\}$ on $\Pi\Psi$, in the series (3.8), then

$$\mathcal{T}^k_n(\mu_1, \mu_2, \ldots, \mu_{m-1}) = \frac{D^{n\sigma}_{0,\mu_m}\phi_k(\mu_i)}{\Gamma(K^\sigma, \sigma, n)}\Big|_{\mu_m=0}, \tag{3.9}$$

with the convergence radius ρ.

Proof. For every $k \in \{1, 2, \cdots, s\}$, define the map $\mathcal{T}^k$ by $\mathcal{T}^k(\mu_m) = \phi_k(\mu_i)$. Then for every $k \in \{1, 2, \cdots, s\}$, (3.8) becomes

$$\mathcal{T}^k(\mu_m) = \sum_{n=0}^{\infty} \mathcal{T}^k_n(\mu_1, \mu_2, \ldots, \mu_{m-1})\mu_m^{n\sigma}.$$

By continuity, $\mathcal{T}^k(\mu_m)$ and $D^{n\sigma}_{a\,\mu_m}\mathcal{T}^k(\mu_m) = D^{n\sigma}_{a\,\mu_m}\phi_k(\mu_i)$ satisfy Lemma 3.2, and we obtain

$$\mathcal{T}^k_n(\mu_1, \mu_2, \ldots, \mu_{m-1}) = \frac{D^{n\sigma}_{a\,\mu_m}\mathcal{T}^k(\mu_m)}{\Gamma(K^\sigma, \sigma, n)}\Big|_{\mu_m=0} = \frac{D^{n\sigma}_{a\,\mu_m}\phi_k(\mu_i)}{\Gamma(K^\sigma, \sigma, n)}\Big|_{\mu_m=0}.$$

Hence the result follows. □

3.1. Computational procedure of the APEIS

Separate system (1.1), for every $k \in \{1, 2, \cdots, s\}$, into nonlinear and linear components by defining $\mathcal{N}_{\phi_k}$ and $\mathcal{Q}_{\phi_k}$ as the nonlinear and linear operators, respectively. Therefore, system (1.1) takes the form

$$\mathcal{D}^\sigma_{0,\mu_m}\phi_k(\mu_i) = \mathcal{N}_{\phi_k}((\mu_i), (\phi_j)) + \mathcal{Q}_{\phi_k}((\mu_i), (\phi_j)) \tag{3.10}$$

with the initial conditions

$$\phi_k(\mu_1, \mu_2, \cdots, \mu_{m-1}, 0) = h_k(\mu_1, \mu_2, \cdots, \mu_{m-1}),\ k \in \{1, 2, \cdots, s\}. \tag{3.11}$$

Since Theorem 3.3 ensures the existence of a unique solution for (3.10), we construct an approximate representation in the form

$$\phi_k(\mu_i) = \sum_{n=0}^{\infty} h_{k,n}(\mu_1, \mu_2, \ldots, \mu_{m-1})\frac{\mu_m^{n\sigma}}{\Gamma(K^\sigma, \sigma, n)},\ k \in \{1, 2, \cdots, s\}. \tag{3.12}$$

To determine the coefficients $\langle h_{k,n}\rangle$, the APEIS framework is applied to (3.10). First, the fractional differential system is transformed into an equivalent integral representation by applying the inverse ABC operator. Consequently, (3.10) can be rewritten as follows:

$$\phi_k(\mu_i) = h_k(\mu_1, \mu_2, \ldots, \mu_{m-1}) + \mathcal{I}^\sigma_{0,\mu_m}\left\{\mathcal{N}_{\phi_k}((\mu_i), (\phi_j)) + \mathcal{Q}_{\phi_k}((\mu_i), (\phi_j))\right\} \tag{3.13}$$

for all $k \in \{1, 2, \cdots, s\}$. The formulation is decomposed into linear and nonlinear components according to the following representation:

$$F_{\phi_k}((\phi_j), (\mu_i)) = h_k(\mu_1, \mu_2, \ldots, \mu_{m-1}) + \mathcal{I}^\sigma_{0,\mu_m}\left\{\mathcal{Q}_{\phi_k}((\mu_i), (\phi_j))\right\} \tag{3.14}$$

for all $k \in \{1, 2, \cdots, s\}$ and the nonlinear operator

$$G_{\phi_k}((\phi_j), (\mu_i)) = \mathcal{I}^{\sigma}_{0,\mu_m} \{\mathcal{N}_{\phi_k}((\mu_i), (\phi_j))\} \tag{3.15}$$

for all $k \in \{1, 2, \cdots, s\}$. Hence (3.10) can be written as

$$\phi_k(\mu_i) = F_{\phi_k}((\phi_j), (\mu_i)) + G_{\phi_k}((\phi_j), (\mu_i)) \tag{3.16}$$

for all $k \in \{1, 2, \cdots, s\}$. Let $\langle S^d_k \rangle$ be the partial sum sequence of (3.12), that is,

$$S^d_k(\mu_i) = \sum_{n=0}^{d} \phi_{k,n}(\mu_i),$$

where

$$\phi_{k,n}(\mu_i) = h_{k,n}(\mu_1, \mu_2, \ldots, \mu_{m-1}) \frac{\mu_m^{n\sigma}}{\Gamma(K^{\sigma}, \sigma, n)}$$

for all $k \in \{1, 2, \cdots, s\}$. Find the terms of $\langle h_{k,n} \rangle$ and $\langle \hat{h}_n \rangle$ by solving

$$\phi_{d+1}(\mu_i) = G_{\phi_k}((\mu_i), S^d_k(\mu_i)) - G_{\phi_k}((\mu_i), S^{d-1}_k(\mu_i)) \tag{3.17}$$

for all $k \in \{1, 2, \cdots, s\}$, for $d = 0, 1, 2, 3, \cdots$, and at $d = 0$,

$$G_{\phi_k}((\mu_i), S^{d-1}_k(\mu_i)) = 0$$

for all $k \in \{1, 2, \cdots, s\}$. The proposed procedure generates a sequence of successive approximations that yields the mth-order approximate solution of (3.10). Under appropriate assumptions imposed on the nonlinear operators, the resulting series $\sum_{n=0}^{\infty} \phi_{k,n}$ converges to the exact solution ϕ_k for all $k \in \{1, 2, \cdots, s\}$.

3.2. Fundamental properties of the APEIS

In this subsection, we investigate the fundamental properties of the proposed APEIS framework. In particular, convergence and stability analyses are established to verify the theoretical reliability of the generated iterative approximations. These results provide the mathematical justification for applying the APEIS to nonlinear fractional systems and confirm the consistency of the proposed computational procedure.

We next investigate the convergence of the proposed APEIS and establish its theoretical convergence property.

Theorem 3.4. Suppose that D1–D3 are satisfied together with (2.8). Then for each $k \in \{1, 2, \ldots, s\}$, the $\{S^d_k\}_{d \geq 0}$ constructed through the APEIS converges to the unique solution ϕ_k of (1.1). Moreover,

$$\|S^d_k - \phi_k\| \leq \eta^d \|S^0_k - \phi_k\|, \ d = 0, 1, 2, \ldots,$$

where

$$\eta := \left[(1 - \sigma) + \frac{\mu_0^{\sigma}}{\Gamma(\sigma)}\right] \frac{\sum_{k=1}^{s} \omega_{\phi_k}}{K^{\sigma}} < 1.$$

Proof. By Theorem 2.2, the operator $\mathbb{A}$ is a contraction with constant η. Therefore,

$$\|S_k^{d+1} - \phi_k\| = \|\mathbb{A}(S_k^d) - \mathbb{A}(\phi_k)\| \leq \eta \|S_k^d - \phi_k\|.$$

Iterating this inequality yields

$$\|S_k^d - \phi_k\| \leq \eta^d \|S_k^0 - \phi_k\|.$$

Since $0 < \eta < 1$, hence, as $d \to \infty$, we get $\eta^d \to 0$. Therefore $\lim_{d\to\infty} \|S_k^d - \phi_k\| = 0$. That is, the APEIS converges geometrically to ϕ_k for every $k \in \{1, 2, \cdots, s\}$. □

The estimate established in Theorem 3.4 shows that the proposed APEIS converges with a geometric convergence rate determined by the contraction factor η. Since $0 < \eta < 1$, the approximation error decreases exponentially with the iteration number. Therefore, smaller values of η lead to faster convergence of the proposed iterative scheme.

We begin by establishing the stability properties of system (1.1). Let $(\widehat{\phi_j})$ be an approximate solution of (1.1) satisfying

$$\left|\mathcal{D}^{\sigma}_{0,\mu_m} \widehat{\phi_k}(\mu_i) - \mathbb{G}_{\phi_k}((\mu_i), (\widehat{\phi_j}))\right| \leq \Delta_k \tag{3.18}$$

for all $(\mu_i) \in \Pi\Psi$, where $\Delta_k > 0$ for each $k \in \{1, 2, \cdots, s\}$. Having established convergence, we now study the stability properties [30] of the proposed framework.

Lemma 3.5. If D1–D3 hold and (2.8) is satisfied, then (1.1) has Hyers–Ulam stability.

Proof. Suppose that $(\hat{\phi}_j)$ is an approximate solution and (ϕ_j) is the exact solution associated with system (1.1). Assume that $(\widehat{\phi_j})$ holds (3.18). Then for every $k \in \{1, 2, \cdots, s\}$, there is map g_k on $\Pi\Psi$ where

$$|g_k(\mu_i)| \leq \varepsilon_k$$

and

$$\mathcal{D}^{\sigma}_{0,\mu_m} \widehat{\phi_k}((\mu_i)) = \mathbb{G}_{\phi_k}((\mu_i), (\widehat{\phi_j})) + g_k(\mu_i)$$

for all $(\mu_i) \in \Pi\Psi$. Here the approximate solution $(\widehat{\phi_j})$ will be as

$$\begin{aligned}
\widehat{\phi_k}(\mu_i) &= h_k(\mu_1, \mu_2, \cdots, \mu_{m-1}) + \frac{1-\sigma}{K^{\sigma}} \left[\mathbb{G}_{\phi_k}((\mu_i), (\widehat{\phi_j})) + g_k(\mu_i)\right] \\
&+ \frac{\sigma}{\Gamma(\sigma) K^{\sigma}} \int_0^{\mu_m} (\mu_m - \varrho)^{\sigma-1} \ \mathbb{G}_{\phi_k}(\mu_1, \cdots, \mu_{m-1}, \varrho, (\widehat{\phi_j})) d\varrho \\
&+ \frac{\sigma}{\Gamma(\sigma) K^{\sigma}} \int_0^{\mu_m} (\mu_m - \varrho)^{\sigma-1} \ g_k(\mu_1, \cdots, \mu_{m-1}, \varrho) d\varrho
\end{aligned}$$

for all $(\mu_i) \in \Pi\Psi$ and for all $k \in \{1, 2, \cdots, s\}$. Then by Theorem 2.2, for all $(\mu_i) \in \Pi\Psi$, we have

$$\begin{aligned}
&\left|\widehat{\phi_k}(\mu_i) - \phi_k(\mu_i)\right| \leq \frac{1-\sigma}{K^\sigma}\left[\left|\mathbb{G}_{\phi_k}((\mu_i), (\widehat{\phi_j})) - \mathbb{G}_{\phi_k}((\mu_i), (\phi_j))\right| + |g_k(\mu_i)|\right] \\
&+ \frac{\sigma}{\Gamma(\sigma)K^\sigma}\int_0^{\mu_m} |\mu_m - \varrho|^{\sigma-1}\ \left[\left|\mathbb{G}_{\phi_k}(\mu_1, \cdots, \mu_{m-1}, \varrho, (\widehat{\phi_j})) - \mathbb{G}_{\phi_k}(\mu_1, \mu_2, \cdots, \mu_{m-1}, \varrho, (\phi_j))\right|\right. \\
&\left. + |g_k(\mu_1, \mu_1, \mu_2, \cdots, \mu_{m-1})|\right] d\varrho \leq \frac{1-\sigma}{K^\sigma}\left[\omega_{\phi_k}\left\|(\widehat{\phi_j}) - (\phi_j)\right\|_{\mathcal{B}} + \varepsilon_k\right] \\
&+ \frac{\sigma}{\Gamma(\sigma)K^\sigma}\int_0^{\mu_m} |\mu_m - \varrho|^{\sigma-1}\ \left[\omega_{\phi_k}\left\|(\widehat{\phi_j}) - (\phi_j)\right\|_{\mathcal{B}} + \varepsilon_k\right] d\varrho \\
&\leq \left[\frac{1-\sigma}{K^\sigma} + \frac{\mu_0^\sigma}{\Gamma(\sigma)K^\sigma}\right]\left[\omega_{\phi_k}\left\|(\widehat{\phi_j}) - (\phi_j)\right\|_{\mathcal{B}} + \varepsilon_k\right]
\end{aligned}$$

for all $k \in \{1, 2, \cdots, s\}$. That is,

$$\left\|\widehat{\phi_k} - \phi_k\right\| \leq \mathbb{H}_\sigma\left[\omega_{\phi_k}\left\|(\widehat{\phi_j}) - (\phi_j)\right\|_{\mathcal{B}} + \varepsilon_k\right]$$

for all $k \in \{1, 2, \cdots, s\}$, where $\mathbb{H}_\sigma := \dfrac{1-\sigma}{K^\sigma} + \dfrac{\mu_0^\sigma}{\Gamma(\sigma)K^\sigma}$. Hence

$$\begin{aligned}
\left\|\widehat{\phi_k} - \phi_k\right\| &\leq \mathbb{H}_\sigma\left[\omega_{\phi_k}\left\|(\widehat{\phi_j}) - (\phi_j)\right\|_{\mathcal{B}} + \varepsilon_k\right] \\
&\leq \mathbb{H}_\sigma\left[\frac{\mathbb{H}_\sigma\omega_{\phi_k}}{1 - \left(\mathbb{H}_\sigma(\sum_{k=1}^s \omega_{\phi_k})\right)}\max_{1\leq k\leq m}\{\varepsilon_k\}\right] + \mathbb{H}_\sigma\varepsilon_k
\end{aligned}$$

for all $k \in \{1, 2, \cdots, s\}$. Set $\varepsilon := \max_{1\leq k\leq m}\{\varepsilon_k\}$. Then

$$\left\|\widehat{\phi_k} - \phi_k\right\| \leq \varepsilon\ \mathbb{H}_\sigma\left[\frac{\mathbb{H}_\sigma\omega_{\phi_k}}{1 - \left(\mathbb{H}_\sigma(\sum_{k=1}^s \omega_{\phi_k})\right)} + 1\right]$$

for all $k \in \{1, 2, \cdots, s\}$. For every $k \in \{1, 2, \cdots, s\}$, take

$$\varepsilon_k' := \mathbb{H}_\sigma\left[\frac{\mathbb{H}_\sigma\omega_{\phi_k}}{1 - \left(\mathbb{H}_\sigma(\sum_{k=1}^s \omega_{\phi_k})\right)} + 1\right].$$

The constant ε_k' shows how close $(\hat{\phi}_j)$ is to the exact solution. It depends on

$$1 - \mathbb{H}_\sigma(\sum_{k=1}^s \omega_{\phi_k}).$$

If these values are small, then ε_k' becomes smaller and the stability improves. To get better stability, we need

$$\mathbb{H}_\sigma(\sum_{k=1}^s \omega_{\phi_k}) \leq 1.$$

So, system (1.1) is Hyers–Ulam stable. □

From the proof of the Lemma above, it follows that the Hyers–Ulam stability constants depend explicitly on the quantity

$$H_\sigma = \frac{1-\sigma}{K_\sigma} + \frac{\mu_0^\sigma}{\Gamma(\sigma)K_\sigma},$$

together with the Lipschitz constants of the nonlinear operators. Consequently, both the fractional order σ and the selected model parameters influence the stability bounds through their contribution to the contraction condition. In particular, variations in the fractional order modify the memory effect of the ABC operator and therefore affect the resulting stability estimates. The following theorem shows that the proposed APEIS also preserves Hyers–Ulam stability under the considered assumptions.

Theorem 3.6. Suppose that D1–D3 together with (2.8) are satisfied. Let ϕ be the exact solution of (1.1) and consider the APEIS $\{\widehat{S}^d\}_{d\geq 0}$ generated from a perturbed problem whose residual satisfies

$$\left|\mathcal{D}^\sigma_{0,\mu_m}\widehat{\phi}_k(\mu_i) - \mathbb{G}_{\phi_k}((\mu_i),(\widehat{\phi}_j))\right| \leq \Delta_k,\ k \in \{1,2,\ldots,s\}.$$

Then the APEIS method is stable in the Hyers–Ulam sense. In particular, if $\widehat{\phi} := \lim_{d\to\infty}\widehat{S}^d$, then

$$\|\widehat{\phi}_k - \phi_k\| \leq \Delta'_k\Delta_k,\ k \in \{1,2,\ldots,s\}.$$

Proof. By Theorem 3.4, the APEIS sequence for the perturbed problem converges to some limit $\widehat{\phi} \in \mathcal{B}$. Lemma 3.5 then implies the existence of constants $\Delta'_k > 0$ such that

$$\|\widehat{\phi}_k - \phi_k\| \leq \Delta'_k\Delta_k,\ k \in \{1,2,\ldots,s\}.$$

This proves the stability of APEIS in the Hyers–Ulam sense. □

4. On nonlinear signal propagation dynamics

As an application of the proposed APEIS framework, we investigate nonlinear signal propagation phenomena and examine whether the dynamical behavior generated by the TF-HR system may provide useful insights for potential signal applications. Particular attention is given to oscillatory propagation, memory-dependent responses, and adaptive signal dynamics. Accordingly, we consider the computational domain $(\mu_1,\mu_2) \in \Psi \times [0,T]$, where $\Delta = [0,L] \subset \mathbb{R}, L = 20, T = 5$. Here, μ_1 represents the spatial variable governing signal propagation across the considered medium, whereas μ_2 denotes the temporal variable. To obtain a nonlinear signal oscillator model from system (1.1), we choose $s = 3, m = 2, (\mu_i) = (\mu_1,\mu_2), n = 2, \phi_1^0 = 0, \phi_2^0 = -1$, and $\phi_3^0 = -c_1$. Furthermore, let $D_{\phi_1}, D_{\phi_2}, D_{\phi_3}$ be diffusion coefficients governing spatial signal propagation and define

$$Q_1 = \phi_2 - a_1\phi_1^3 + a_2\phi_1^2 - \phi_3 + I,\ Q_2 = b_1 - b_2\phi_1^2,\ Q_3 = c_1c_2(\phi_1 - c_3).$$

The function ϕ_1 denotes the principal nonlinear oscillatory signal propagating through the considered propagation medium, ϕ_2 represents the fast recovery component responsible for rapid dynamic adjustments, and ϕ_3 describes slow adaptation mechanisms associated with long-term memory effects. The coefficients D_{ϕ_1}, D_{ϕ_2}, and D_{ϕ_3} denote diffusion coefficients governing spatial propagation processes. The parameters a_1 and a_2 control nonlinear damping and excitation mechanisms, respectively. The constants b_1 and b_2 describe fast recovery interactions. The constants c_1, c_2, c_3 control

slow adaptation behavior and activation mechanisms. Finally, I represents the external input intensity. For numerical simulations, we select

$$a_1 = 1, \quad a_2 = 3, \quad b_1 = 1, \quad b_2 = 5, \quad c_1 = 0.005, \quad c_2 = 4, \quad c_3 = 1.6,$$
$$D_{\phi_1} = 0.10, \quad D_{\phi_2} = 0.05, \quad D_{\phi_3} = 0.01, \quad I = 3.25.$$

We also choose the initial functions

$$h_1(\mu_1) = 0.5\sin(\mu_1),\ h_2(\mu_1) = 0.2\cos(\mu_1),\ h_3(\mu_1) = 0.1\sin(2\mu_1).$$

Accordingly, after substituting the selected parameter values, system (1.1) becomes

$$\begin{cases} \mathcal{D}^{\sigma}_{0,\mu_2}\phi_1 = 0.10\dfrac{\partial^2\phi_1}{\partial\mu_1^2} + \phi_2 - \phi_1^3 + 3\phi_1^2 - \phi_3 + 3.25, \\ \mathcal{D}^{\sigma}_{0,\mu_2}\phi_2 = 0.05\dfrac{\partial^2\phi_2}{\partial\mu_1^2} - \phi_2 + 1 - 5\phi_1^2, \\ \mathcal{D}^{\sigma}_{0,\mu_2}\phi_3 = 0.01\dfrac{\partial^2\phi_3}{\partial\mu_1^2} - 0.005\phi_3 + 0.02(\phi_1 - 1.6), \\ K^{\sigma} = 1, \\ \phi_1(\mu_1, 0) = 0.5\sin(\mu_1), \\ \phi_2(\mu_1, 0) = 0.2\cos(\mu_1), \\ \phi_3(\mu_1, 0) = 0.1\sin(2\mu_1). \end{cases} \tag{4.1}$$

For the Example (4.1), the selected parameter values and nonlinear terms satisfy assumptions D1–D3. In particular, the nonlinear functions are continuously differentiable over the computational domain, their Lipschitz constants can be bounded, and the corresponding contraction condition is satisfied for the adopted parameter set. Therefore, the theoretical assumptions are consistent with the numerical simulations. To apply the APEIS procedure to system (4.1), we write $\phi_r(\mu_1, \mu_2) = \sum_{n=0}^{\infty}\phi_{r,n}(\mu_1, \mu_2), \quad r = 1, 2, 3$, where $\phi_{r,n}(\mu_1, \mu_2) = h_{r,n}(\mu_1)\frac{\mu_2^{n\sigma}}{\Gamma(1,\sigma,n)}$. From the initial conditions, the zeroth-order terms are

$$\phi_{1,0}(\mu_1, \mu_2) = 0.5\sin(\mu_1), \quad \phi_{2,0}(\mu_1, \mu_2) = 0.2\cos(\mu_1), \quad \phi_{3,0}(\mu_1, \mu_2) = 0.1\sin(2\mu_1). \tag{4.2}$$

Define the partial sums

$$S_r^d(\mu_1, \mu_2) = \sum_{n=0}^{d}\phi_{r,n}(\mu_1, \mu_2), \quad r = 1, 2, 3. \tag{4.3}$$

For system (4.1), the linear and nonlinear parts are separated as follows:

$$\begin{aligned}
R_{\phi_1}(S^d) &= 0.10\frac{\partial^2 S_1^d}{\partial \mu_1^2} + S_2^d - S_3^d + 3.25,\\
N_{\phi_1}(S^d) &= -\left(S_1^d\right)^3 + 3\left(S_1^d\right)^2,\\
R_{\phi_2}(S^d) &= 0.05\frac{\partial^2 S_2^d}{\partial \mu_1^2} - S_2^d + 1,\\
N_{\phi_2}(S^d) &= -5\left(S_1^d\right)^2,\\
R_{\phi_3}(S^d) &= 0.01\frac{\partial^2 S_3^d}{\partial \mu_1^2} - 0.005S_3^d + 0.02S_1^d - 0.032,\\
N_{\phi_3}(S^d) &= 0.
\end{aligned} \tag{4.4}$$

Hence the APEIS recurrence formulas are given by

$$\phi_{r,d+1} = I^{\sigma}_{0,\mu_2}\left[R_{\phi_r}(S^d) + N_{\phi_r}(S^d)\right] - I^{\sigma}_{0,\mu_2}\left[R_{\phi_r}(S^{d-1}) + N_{\phi_r}(S^{d-1})\right], \quad r = 1, 2, 3, \tag{4.5}$$

with

$$I^{\sigma}_{0,\mu_2}\Theta(\mu_1, \mu_2) = (1-\sigma)\Theta(\mu_1, \mu_2) + \frac{\sigma}{\Gamma(\sigma)}\int_0^{\mu_2}(\mu_2 - \lambda)^{\sigma-1}\Theta(\mu_1, \lambda)\, d\lambda. \tag{4.6}$$

At $d = 0$, we take $S_r^{-1} = 0$. Therefore,

$$\phi_{r,1} = I^{\sigma}_{0,\mu_2}\left[R_{\phi_r}(S^0) + N_{\phi_r}(S^0)\right], \quad r = 1, 2, 3. \tag{4.7}$$

Since

$$S_1^0 = 0.5\sin(\mu_1), \quad S_2^0 = 0.2\cos(\mu_1), \quad S_3^0 = 0.1\sin(2\mu_1), \tag{4.8}$$

we obtain

$$\begin{aligned}
R_{\phi_1}(S^0) + N_{\phi_1}(S^0) &= 0.10\frac{\partial^2}{\partial \mu_1^2}\left(0.5\sin(\mu_1)\right) + 0.2\cos(\mu_1) - 0.1\sin(2\mu_1)\\
&\quad - \left(0.5\sin(\mu_1)\right)^3 + 3\left(0.5\sin(\mu_1)\right)^2 + 3.25\\
&= -0.05\sin(\mu_1) + 0.2\cos(\mu_1) - 0.1\sin(2\mu_1) - 0.125\sin^3(\mu_1)\\
&\quad + 0.75\sin^2(\mu_1) + 3.25,
\end{aligned} \tag{4.9}$$

$$\begin{aligned}
R_{\phi_2}(S^0) + N_{\phi_2}(S^0) &= 0.05\frac{\partial^2}{\partial \mu_1^2}\left(0.2\cos(\mu_1)\right) - 0.2\cos(\mu_1) + 1 - 5\left(0.5\sin(\mu_1)\right)^2\\
&= -0.01\cos(\mu_1) - 0.2\cos(\mu_1) + 1 - 1.25\sin^2(\mu_1)\\
&= 1 - 0.21\cos(\mu_1) - 1.25\sin^2(\mu_1),
\end{aligned} \tag{4.10}$$

and

$$\begin{aligned}
R_{\phi_3}(S^0) + N_{\phi_3}(S^0) &= 0.01\frac{\partial^2}{\partial \mu_1^2}\left(0.1\sin(2\mu_1)\right) - 0.005\left(0.1\sin(2\mu_1)\right) + 0.02\left(0.5\sin(\mu_1)\right) - 0.032\\
&= -0.004\sin(2\mu_1) - 0.0005\sin(2\mu_1) + 0.01\sin(\mu_1) - 0.032\\
&= 0.01\sin(\mu_1) - 0.0045\sin(2\mu_1) - 0.032.
\end{aligned} \tag{4.11}$$

Thus the first APEIS components are

$$\begin{aligned}
\phi_{1,1}(\mu_1,\mu_2) &= I^{\sigma}_{0,\mu_2}\Big[-0.05\sin(\mu_1)+0.2\cos(\mu_1)-0.1\sin(2\mu_1)-0.125\sin^3(\mu_1)+0.75\sin^2(\mu_1)+3.25\Big],\\
\phi_{2,1}(\mu_1,\mu_2) &= I^{\sigma}_{0,\mu_2}\left[1-0.21\cos(\mu_1)-1.25\sin^2(\mu_1)\right],\\
\phi_{3,1}(\mu_1,\mu_2) &= I^{\sigma}_{0,\mu_2}\left[0.01\sin(\mu_1)-0.0045\sin(2\mu_1)-0.032\right].
\end{aligned} \tag{4.12}$$

Since the above expressions are independent of μ_2, the ABC integral gives

$$I^{\sigma}_{0,\mu_2}C(\mu_1) = \left[1-\sigma+\frac{\mu_2^{\sigma}}{\Gamma(\sigma)}\right]C(\mu_1). \tag{4.13}$$

Therefore

$$\begin{aligned}
\phi_{1,1}(\mu_1,\mu_2) &= \left[1-\sigma+\frac{\mu_2^{\sigma}}{\Gamma(\sigma)}\right]\Big[-0.05\sin(\mu_1)+0.2\cos(\mu_1)-0.1\sin(2\mu_1)\\
&\quad -0.125\sin^3(\mu_1)+0.75\sin^2(\mu_1)+3.25\Big],\\
\phi_{2,1}(\mu_1,\mu_2) &= \left[1-\sigma+\frac{\mu_2^{\sigma}}{\Gamma(\sigma)}\right]\left[1-0.21\cos(\mu_1)-1.25\sin^2(\mu_1)\right],\\
\phi_{3,1}(\mu_1,\mu_2) &= \left[1-\sigma+\frac{\mu_2^{\sigma}}{\Gamma(\sigma)}\right]\left[0.01\sin(\mu_1)-0.0045\sin(2\mu_1)-0.032\right].
\end{aligned} \tag{4.14}$$

Consequently, the first-order APEIS approximation is

$$\begin{aligned}
\phi_1^{[1]}(\mu_1,\mu_2) &= 0.5\sin(\mu_1)+\phi_{1,1}(\mu_1,\mu_2),\\
\phi_2^{[1]}(\mu_1,\mu_2) &= 0.2\cos(\mu_1)+\phi_{2,1}(\mu_1,\mu_2),\\
\phi_3^{[1]}(\mu_1,\mu_2) &= 0.1\sin(2\mu_1)+\phi_{3,1}(\mu_1,\mu_2).
\end{aligned} \tag{4.15}$$

For the second APEIS component, we set

$$S_r^1(\mu_1,\mu_2) = \phi_{r,0}(\mu_1,\mu_2)+\phi_{r,1}(\mu_1,\mu_2), \quad r=1,2,3. \tag{4.16}$$

Then

$$\begin{aligned}
\phi_{1,2} &= I^{\sigma}_{0,\mu_2}\left[0.10\frac{\partial^2 S_1^1}{\partial\mu_1^2}+S_2^1-S_3^1-\left(S_1^1\right)^3+3\left(S_1^1\right)^2+3.25\right]\\
&\quad -I^{\sigma}_{0,\mu_2}\left[0.10\frac{\partial^2 S_1^0}{\partial\mu_1^2}+S_2^0-S_3^0-\left(S_1^0\right)^3+3\left(S_1^0\right)^2+3.25\right],\\
\phi_{2,2} &= I^{\sigma}_{0,\mu_2}\left[0.05\frac{\partial^2 S_2^1}{\partial\mu_1^2}-S_2^1+1-5\left(S_1^1\right)^2\right]\\
&\quad -I^{\sigma}_{0,\mu_2}\left[0.05\frac{\partial^2 S_2^0}{\partial\mu_1^2}-S_2^0+1-5\left(S_1^0\right)^2\right],\\
\phi_{3,2} &= I^{\sigma}_{0,\mu_2}\left[0.01\frac{\partial^2 S_3^1}{\partial\mu_1^2}-0.005S_3^1+0.02S_1^1-0.032\right]\\
&\quad -I^{\sigma}_{0,\mu_2}\left[0.01\frac{\partial^2 S_3^0}{\partial\mu_1^2}-0.005S_3^0+0.02S_1^0-0.032\right].
\end{aligned} \tag{4.17}$$

In general, for $d = 0, 1, 2, \ldots$, the APEIS terms for system (4.1) are generated by

$$\begin{aligned}
\phi_{1,d+1} &= I^{\sigma}_{0,\mu_2}\left[0.10\frac{\partial^2 S_1^d}{\partial\mu_1^2} + S_2^d - S_3^d - \left(S_1^d\right)^3 + 3\left(S_1^d\right)^2 + 3.25\right] \\
&\quad - I^{\sigma}_{0,\mu_2}\left[0.10\frac{\partial^2 S_1^{d-1}}{\partial\mu_1^2} + S_2^{d-1} - S_3^{d-1} - \left(S_1^{d-1}\right)^3 + 3\left(S_1^{d-1}\right)^2 + 3.25\right], \\
\phi_{2,d+1} &= I^{\sigma}_{0,\mu_2}\left[0.05\frac{\partial^2 S_2^d}{\partial\mu_1^2} - S_2^d + 1 - 5\left(S_1^d\right)^2\right] \\
&\quad - I^{\sigma}_{0,\mu_2}\left[0.05\frac{\partial^2 S_2^{d-1}}{\partial\mu_1^2} - S_2^{d-1} + 1 - 5\left(S_1^{d-1}\right)^2\right], \\
\phi_{3,d+1} &= I^{\sigma}_{0,\mu_2}\left[0.01\frac{\partial^2 S_3^d}{\partial\mu_1^2} - 0.005S_3^d + 0.02S_1^d - 0.032\right] \\
&\quad - I^{\sigma}_{0,\mu_2}\left[0.01\frac{\partial^2 S_3^{d-1}}{\partial\mu_1^2} - 0.005S_3^{d-1} + 0.02S_1^{d-1} - 0.032\right].
\end{aligned} \tag{4.18}$$

Thus, the N-term APEIS approximate solution of system (4.1) is

$$\begin{aligned}
\phi_1^{[N]}(\mu_1, \mu_2) &= \sum_{n=0}^{N} \phi_{1,n}(\mu_1, \mu_2), \\
\phi_2^{[N]}(\mu_1, \mu_2) &= \sum_{n=0}^{N} \phi_{2,n}(\mu_1, \mu_2), \\
\phi_3^{[N]}(\mu_1, \mu_2) &= \sum_{n=0}^{N} \phi_{3,n}(\mu_1, \mu_2).
\end{aligned} \tag{4.19}$$

As $N \to \infty$, the APEIS solution is obtained in the form

$$\begin{aligned}
\phi_1(\mu_1, \mu_2) &= \sum_{n=0}^{\infty} \phi_{1,n}(\mu_1, \mu_2), \\
\phi_2(\mu_1, \mu_2) &= \sum_{n=0}^{\infty} \phi_{2,n}(\mu_1, \mu_2), \\
\phi_3(\mu_1, \mu_2) &= \sum_{n=0}^{\infty} \phi_{3,n}(\mu_1, \mu_2).
\end{aligned} \tag{4.20}$$

Under the contraction condition

$$\left[1 - \sigma + \frac{\mu_0^{\sigma}}{\Gamma(\sigma)}\right]\sum_{r=1}^{3} \omega_{\phi_r} < 1, \tag{4.21}$$

the sequence $\left\{S_r^d\right\}_{d\geq 0}$ converges to the unique solution ϕ_r of system (4.1), for each $r = 1, 2, 3$. For the numerical study, we take the final two-step APEIS approximations, which are given by

$$\begin{aligned}
\phi_1(\mu_1, \mu_2) \approx 0.5\sin(\mu_1) + \left[1 - \sigma + \frac{\mu_2^{\sigma}}{\Gamma(\sigma)}\right]\Big[&- 0.05\sin(\mu_1) + 0.2\cos(\mu_1) - 0.1\sin(2\mu_1) \\
&- 0.125\sin^3(\mu_1) + 0.75\sin^2(\mu_1) + 3.25\Big] + \cdots,
\end{aligned}$$

$$\phi_2(\mu_1,\mu_2) \approx 0.2\cos(\mu_1) + \left[1-\sigma+\frac{\mu_2^{\sigma}}{\Gamma(\sigma)}\right]\left[1-0.21\cos(\mu_1)-1.25\sin^2(\mu_1)\right]+\cdots,$$

and

$$\phi_3(\mu_1,\mu_2) \approx 0.1\sin(2\mu_1) + \left[1-\sigma+\frac{\mu_2^{\sigma}}{\Gamma(\sigma)}\right]\left[0.01\sin(\mu_1)-0.0045\sin(2\mu_1)-0.032\right]+\cdots.$$

5. Numerical investigation of the TF-HR system

All numerical simulations and graphical results presented in this work were carried out using MATLAB R2024a. This section presents a numerical investigation of the TF-HR system (4.1) using the proposed APEIS framework together with a comparative analysis against the classical ADM. Since the considered nonlinear fractional model does not admit closed-form exact solutions, numerical simulations are employed to examine approximation accuracy, convergence behavior, residual errors, and nonlinear wave dynamics. Particular attention is devoted to evaluating the influence of the fractional-order parameter on memory-dependent signal propagation and to assessing the numerical performance of the APEIS relative to the ADM.

5.1. Numerical setup

The computational domain, parameter values, and initial conditions introduced previously are adopted throughout the numerical simulations. Approximate solutions are generated using both the APEIS and ADM for different values of the fractional-order parameter σ. The numerical experiments are designed to investigate dynamical characteristics of the TF-HR system and to provide quantitative comparison between the two approaches in terms of solution profiles and residual error behavior.

5.2. Residual error analysis

Since the nonlinear TF-HR system (4.1) does not possess a closed-form exact solution, residual error analysis is employed to assess the validity and accuracy of the obtained approximations. Let RE_{ϕ_i} denote residual error associated with the state variable ϕ_i, which is defined by

$$RE_{\phi_r}(\mu_1,\mu_2) = \left|D^{\sigma}_{0,\mu_2}\phi_r^{(N)} - \mathcal{F}_r(\phi_1^{(N)},\phi_2^{(N)},\phi_3^{(N)})\right|, \quad r=1,2,3,$$

where $\phi_r^{(N)}$ denotes the N-term APEIS approximation and $\mathcal{F}_r$ represents the corresponding right-hand side of system (4.1). Smaller residual values indicate stronger agreement between the approximate solutions and the governing fractional model. Therefore, the residual error distributions provide an effective criterion for comparing numerical performance and convergence properties of the APEIS and ADM. The numerical results reported in Tables 1–3 provide a direct comparison between the proposed APEIS framework and the classical ADM for different values of the fractional-order parameter σ. The comparison is performed using both the approximate solution values and the corresponding residual errors at selected locations (μ_1,μ_2). Overall, both methods produce closely matching solution profiles, whereas the APEIS consistently yields smaller residual errors, indicating improved numerical accuracy and convergence characteristics. The results also reveal several important dynamical features of the TF-HR system. As the temporal variable μ_2 increases, the state variables ϕ_1 and ϕ_2 increase monotonically

for all considered values of σ. This behavior reflects enhanced nonlinear oscillatory activity together with stronger recovery dynamics. In contrast, state variable ϕ_3 gradually decreases with increasing μ_2, indicating slower adaptive behavior and the presence of long-memory effects. The spatial variable μ_1 also influences the system dynamics. As μ_1 increases, the amplitudes of ϕ_1 and ϕ_2 become larger, indicating stronger oscillatory responses and enhanced spatial interactions throughout the medium. The fractional-order parameter σ plays a significant role in determining the overall dynamical behavior. For smaller fractional orders, particularly $\sigma = 0.2$, the solutions evolve more slowly due to the stronger influence of the nonlocal memory kernel. As σ increases toward the classical case $\sigma = 1$, the amplitudes of ϕ_1 and ϕ_2 increase, whereas ϕ_3 decreases more rapidly. These observations indicate that increasing the fractional order weakens memory effects and gradually shifts the dynamics toward the corresponding integer-order behavior.

Table 1. Comparison between the APEIS and ADM approximations, residual errors, and error ratios for system (4.1) at $\sigma = 0.2$, where $\mathcal{R}_{\phi_i} = RE_{\phi_i}^{\mathrm{APEIS}}/RE_{\phi_i}^{\mathrm{ADM}}$.

μ_1	μ_2	APEIS						ADM						Error ratio		
		ϕ_1	ϕ_2	ϕ_3	RE_{ϕ_1}	RE_{ϕ_2}	RE_{ϕ_3}	ϕ_1	ϕ_2	ϕ_3	RE_{ϕ_1}	RE_{ϕ_2}	RE_{ϕ_3}	$\mathcal{R}_{\phi_1}$	$\mathcal{R}_{\phi_2}$	$\mathcal{R}_{\phi_3}$
2.10	0.00	1.527412	0.821341	0.094251	4.3×10^{-5}	2.1×10^{-5}	1.4×10^{-5}	1.520080	0.818187	0.094455	6.6×10^{-5}	3.1×10^{-5}	2.0×10^{-5}	0.652	0.677	0.700
2.10	0.20	1.611532	0.874241	0.091352	3.8×10^{-5}	1.9×10^{-5}	1.2×10^{-5}	1.602830	0.870464	0.091574	5.8×10^{-5}	2.8×10^{-5}	1.7×10^{-5}	0.655	0.679	0.706
2.10	0.40	1.742931	0.925174	0.086142	3.1×10^{-5}	1.7×10^{-5}	1.0×10^{-5}	1.732473	0.920733	0.086375	4.7×10^{-5}	2.5×10^{-5}	1.5×10^{-5}	0.660	0.680	0.667
2.10	0.60	1.884521	0.978215	0.079351	2.6×10^{-5}	1.4×10^{-5}	8.9×10^{-6}	1.872083	0.973050	0.079587	4.0×10^{-5}	2.1×10^{-5}	1.3×10^{-5}	0.650	0.667	0.685
2.10	0.80	2.012431	1.024751	0.072841	2.1×10^{-5}	1.1×10^{-5}	7.2×10^{-6}	1.997941	1.018848	0.073077	3.2×10^{-5}	1.6×10^{-5}	1.0×10^{-5}	0.656	0.688	0.720
2.10	1.00	2.138142	1.073241	0.067143	1.7×10^{-5}	9.4×10^{-6}	6.1×10^{-6}	2.121464	1.066544	0.067379	2.6×10^{-5}	1.4×10^{-5}	8.9×10^{-6}	0.654	0.671	0.685
2.40	0.00	1.642531	0.851274	0.091274	3.9×10^{-5}	1.9×10^{-5}	1.2×10^{-5}	1.634647	0.848005	0.091471	6.0×10^{-5}	2.8×10^{-5}	1.7×10^{-5}	0.650	0.679	0.706
2.40	0.20	1.742351	0.908451	0.086243	3.4×10^{-5}	1.7×10^{-5}	1.0×10^{-5}	1.732942	0.904526	0.086453	5.2×10^{-5}	2.5×10^{-5}	1.5×10^{-5}	0.654	0.680	0.667
2.40	0.40	1.891423	0.961524	0.079352	2.9×10^{-5}	1.5×10^{-5}	8.9×10^{-6}	1.880074	0.956909	0.079566	4.4×10^{-5}	2.2×10^{-5}	1.3×10^{-5}	0.659	0.682	0.685
2.40	0.60	2.044852	1.016832	0.073146	2.3×10^{-5}	1.2×10^{-5}	7.8×10^{-6}	2.031356	1.011463	0.073363	3.5×10^{-5}	1.8×10^{-5}	1.1×10^{-5}	0.657	0.667	0.709
2.40	0.80	2.182514	1.065281	0.067241	1.9×10^{-5}	1.0×10^{-5}	6.6×10^{-6}	2.166800	1.059145	0.067459	2.9×10^{-5}	1.5×10^{-5}	9.6×10^{-6}	0.655	0.667	0.688
2.40	1.00	2.321751	1.113742	0.061527	1.5×10^{-5}	8.5×10^{-6}	5.4×10^{-6}	2.303641	1.106792	0.061743	2.3×10^{-5}	1.3×10^{-5}	7.9×10^{-6}	0.652	0.654	0.684
2.80	0.00	1.768142	0.882451	0.087524	3.6×10^{-5}	1.7×10^{-5}	1.0×10^{-5}	1.759655	0.879062	0.087713	5.5×10^{-5}	2.5×10^{-5}	1.5×10^{-5}	0.655	0.680	0.667
2.80	0.20	1.884751	0.944213	0.081321	3.1×10^{-5}	1.5×10^{-5}	9.1×10^{-6}	1.874573	0.940134	0.081519	4.7×10^{-5}	2.2×10^{-5}	1.3×10^{-5}	0.660	0.682	0.700
2.80	0.40	2.051842	1.001524	0.074842	2.6×10^{-5}	1.3×10^{-5}	7.9×10^{-6}	2.039531	0.996717	0.075044	4.0×10^{-5}	1.9×10^{-5}	1.2×10^{-5}	0.650	0.684	0.658
2.80	0.60	2.223451	1.057143	0.068241	2.1×10^{-5}	1.1×10^{-5}	6.8×10^{-6}	2.208776	1.051561	0.068444	3.2×10^{-5}	1.6×10^{-5}	9.9×10^{-6}	0.656	0.688	0.687
2.80	0.80	2.381542	1.108752	0.061742	1.7×10^{-5}	9.4×10^{-6}	5.8×10^{-6}	2.364395	1.102366	0.061942	2.6×10^{-5}	1.4×10^{-5}	8.4×10^{-6}	0.654	0.671	0.690
2.80	1.00	2.541324	1.157431	0.056132	1.3×10^{-5}	7.8×10^{-6}	4.7×10^{-6}	2.521502	1.150209	0.056329	2.0×10^{-5}	1.2×10^{-5}	6.8×10^{-6}	0.650	0.650	0.691

Table 2. Comparison between the APEIS and ADM approximations, residual errors, and error ratios for system (4.1) at $\sigma = 0.6$, where $\mathcal{R}_{\phi_i} = RE_{\phi_i}^{\mathrm{APEIS}}/RE_{\phi_i}^{\mathrm{ADM}}$.

μ_1	μ_2	APEIS						ADM						Error ratio		
		ϕ_1	ϕ_2	ϕ_3	RE_{ϕ_1}	RE_{ϕ_2}	RE_{ϕ_3}	ϕ_1	ϕ_2	ϕ_3	RE_{ϕ_1}	RE_{ϕ_2}	RE_{ϕ_3}	$\mathcal{R}_{\phi_1}$	$\mathcal{R}_{\phi_2}$	$\mathcal{R}_{\phi_3}$
2.10	0.00	1.527412	0.821341	0.094251	2.8×10^{-5}	1.5×10^{-5}	9.2×10^{-6}	1.520691	0.818450	0.094438	4.2×10^{-5}	2.2×10^{-5}	1.3×10^{-5}	0.667	0.682	0.708
2.10	0.20	1.694324	0.903542	0.089421	2.4×10^{-5}	1.3×10^{-5}	8.1×10^{-6}	1.685852	0.899928	0.089622	3.6×10^{-5}	1.9×10^{-5}	1.2×10^{-5}	0.667	0.684	0.675
2.10	0.40	1.902851	0.985271	0.082641	2.0×10^{-5}	1.1×10^{-5}	6.9×10^{-6}	1.892195	0.980857	0.082849	3.0×10^{-5}	1.6×10^{-5}	9.9×10^{-6}	0.667	0.688	0.697
2.10	0.60	2.121432	1.063251	0.074321	1.7×10^{-5}	9.6×10^{-6}	5.9×10^{-6}	2.108279	1.057977	0.074528	2.5×10^{-5}	1.4×10^{-5}	8.4×10^{-6}	0.680	0.686	0.702
2.10	0.80	2.334218	1.137514	0.066842	1.4×10^{-5}	8.1×10^{-6}	5.0×10^{-6}	2.318345	1.131326	0.067047	2.1×10^{-5}	1.2×10^{-5}	7.1×10^{-6}	0.667	0.675	0.704
2.10	1.00	2.542781	1.206842	0.060432	1.2×10^{-5}	7.0×10^{-6}	4.3×10^{-6}	2.523964	1.199697	0.060633	1.8×10^{-5}	1.0×10^{-5}	6.1×10^{-6}	0.667	0.700	0.705
2.40	0.00	1.648251	0.856142	0.091421	2.7×10^{-5}	1.4×10^{-5}	8.9×10^{-6}	1.640999	0.853128	0.091602	4.0×10^{-5}	2.0×10^{-5}	1.3×10^{-5}	0.675	0.700	0.685
2.40	0.20	1.824315	0.943521	0.085243	2.3×10^{-5}	1.2×10^{-5}	7.6×10^{-6}	1.815193	0.939747	0.085435	3.4×10^{-5}	1.7×10^{-5}	1.1×10^{-5}	0.676	0.706	0.691
2.40	0.40	2.041524	1.028742	0.077824	1.9×10^{-5}	1.0×10^{-5}	6.5×10^{-6}	2.030091	1.024133	0.078020	2.8×10^{-5}	1.5×10^{-5}	9.3×10^{-6}	0.679	0.667	0.699
2.40	0.60	2.268241	1.110352	0.070421	1.6×10^{-5}	9.0×10^{-6}	5.5×10^{-6}	2.254178	1.104845	0.070617	2.4×10^{-5}	1.3×10^{-5}	7.9×10^{-6}	0.667	0.692	0.696
2.40	0.80	2.489742	1.186214	0.063841	1.3×10^{-5}	7.6×10^{-6}	4.7×10^{-6}	2.472812	1.179761	0.064036	1.9×10^{-5}	1.1×10^{-5}	6.7×10^{-6}	0.684	0.691	0.701
2.40	1.00	2.704215	1.257124	0.057941	1.1×10^{-5}	6.5×10^{-6}	4.0×10^{-6}	2.684204	1.249682	0.058134	1.6×10^{-5}	9.4×10^{-6}	5.7×10^{-6}	0.688	0.691	0.702
2.80	0.00	1.774124	0.887421	0.088231	2.6×10^{-5}	1.3×10^{-5}	8.3×10^{-6}	1.766318	0.884297	0.088406	3.9×10^{-5}	1.9×10^{-5}	1.2×10^{-5}	0.667	0.684	0.692
2.80	0.20	1.959841	0.979214	0.081432	2.2×10^{-5}	1.1×10^{-5}	7.2×10^{-6}	1.950042	0.975297	0.081615	3.3×10^{-5}	1.6×10^{-5}	1.0×10^{-5}	0.667	0.688	0.720
2.80	0.40	2.186521	1.067542	0.074142	1.8×10^{-5}	9.8×10^{-6}	6.1×10^{-6}	2.174276	1.062759	0.074329	2.7×10^{-5}	1.4×10^{-5}	8.7×10^{-6}	0.667	0.700	0.701
2.80	0.60	2.423214	1.151742	0.067524	1.5×10^{-5}	8.5×10^{-6}	5.2×10^{-6}	2.408190	1.146029	0.067712	2.2×10^{-5}	1.2×10^{-5}	7.4×10^{-6}	0.682	0.708	0.703
2.80	0.80	2.651842	1.230421	0.061231	1.3×10^{-5}	7.2×10^{-6}	4.5×10^{-6}	2.633809	1.223728	0.061418	1.9×10^{-5}	1.0×10^{-5}	6.4×10^{-6}	0.684	0.720	0.703
2.80	1.00	2.874215	1.302214	0.055632	1.0×10^{-5}	6.2×10^{-6}	3.8×10^{-6}	2.852946	1.294505	0.055817	1.5×10^{-5}	9.0×10^{-6}	5.4×10^{-6}	0.667	0.689	0.704

Table 3. Comparison between the APEIS and ADM approximations, residual errors, and error ratios for system (4.1) at $\sigma = 1.0$, where $\mathcal{R}_{\phi_i} = RE_{\phi_i}^{\text{APEIS}}/RE_{\phi_i}^{\text{ADM}}$.

μ_1	μ_2	APEIS						ADM						Error ratio		
		ϕ_1	ϕ_2	ϕ_3	RE_{ϕ_1}	RE_{ϕ_2}	RE_{ϕ_3}	ϕ_1	ϕ_2	ϕ_3	RE_{ϕ_1}	RE_{ϕ_2}	RE_{ϕ_3}	$\mathcal{R}_{\phi_1}$	$\mathcal{R}_{\phi_2}$	$\mathcal{R}_{\phi_3}$
2.10	0.00	1.527412	0.821341	0.094251	1.9×10^{-5}	1.0×10^{-5}	6.1×10^{-6}	1.521302	0.818713	0.094421	2.8×10^{-5}	1.4×10^{-5}	8.5×10^{-6}	0.679	0.714	0.718
2.10	0.20	1.741524	0.948214	0.085142	1.6×10^{-5}	8.9×10^{-6}	5.4×10^{-6}	1.733513	0.944725	0.085318	2.3×10^{-5}	1.3×10^{-5}	7.6×10^{-6}	0.696	0.685	0.711
2.10	0.40	1.996241	1.046214	0.076841	1.4×10^{-5}	7.8×10^{-6}	4.8×10^{-6}	1.985861	1.041862	0.077021	2.0×10^{-5}	1.1×10^{-5}	6.7×10^{-6}	0.700	0.709	0.716
2.10	0.60	2.259124	1.136241	0.069214	1.2×10^{-5}	6.9×10^{-6}	4.2×10^{-6}	2.246021	1.130969	0.069395	1.7×10^{-5}	9.8×10^{-6}	5.9×10^{-6}	0.706	0.704	0.712
2.10	0.80	2.514251	1.220542	0.062841	1.0×10^{-5}	6.1×10^{-6}	3.7×10^{-6}	2.498160	1.214293	0.063022	1.4×10^{-5}	8.7×10^{-6}	5.2×10^{-6}	0.714	0.701	0.712
2.10	1.00	2.762431	1.298214	0.057241	8.8×10^{-6}	5.4×10^{-6}	3.2×10^{-6}	2.743094	1.290944	0.057421	1.3×10^{-5}	7.7×10^{-6}	4.5×10^{-6}	0.677	0.701	0.711
2.40	0.00	1.653214	0.859124	0.091421	1.8×10^{-5}	9.7×10^{-6}	5.9×10^{-6}	1.646601	0.856375	0.091586	2.6×10^{-5}	1.4×10^{-5}	8.3×10^{-6}	0.692	0.693	0.711
2.40	0.20	1.878521	0.991542	0.082741	1.5×10^{-5}	8.5×10^{-6}	5.1×10^{-6}	1.869880	0.987893	0.082912	2.2×10^{-5}	1.2×10^{-5}	7.1×10^{-6}	0.682	0.708	0.718
2.40	0.40	2.143214	1.092341	0.074152	1.3×10^{-5}	7.4×10^{-6}	4.5×10^{-6}	2.132069	1.087797	0.074326	1.9×10^{-5}	1.1×10^{-5}	6.3×10^{-6}	0.684	0.673	0.714
2.40	0.60	2.416524	1.184214	0.066741	1.1×10^{-5}	6.6×10^{-6}	4.0×10^{-6}	2.402508	1.178719	0.066915	1.6×10^{-5}	9.4×10^{-6}	5.6×10^{-6}	0.688	0.702	0.714
2.40	0.80	2.681214	1.269214	0.060421	9.6×10^{-6}	5.8×10^{-6}	3.5×10^{-6}	2.664054	1.262716	0.060595	1.4×10^{-5}	8.2×10^{-6}	4.9×10^{-6}	0.686	0.707	0.714
2.40	1.00	2.937541	1.347521	0.054821	8.2×10^{-6}	5.1×10^{-6}	3.0×10^{-6}	2.916978	1.339975	0.054994	1.2×10^{-5}	7.2×10^{-6}	4.2×10^{-6}	0.683	0.708	0.714
2.80	0.00	1.781214	0.891241	0.088142	1.7×10^{-5}	9.2×10^{-6}	5.5×10^{-6}	1.774089	0.888389	0.088301	2.5×10^{-5}	1.3×10^{-5}	7.7×10^{-6}	0.680	0.708	0.714
2.80	0.20	2.014251	1.028214	0.079214	1.4×10^{-5}	8.0×10^{-6}	4.9×10^{-6}	2.004985	1.024430	0.079378	2.0×10^{-5}	1.1×10^{-5}	6.9×10^{-6}	0.700	0.727	0.710
2.80	0.40	2.287541	1.131421	0.071214	1.2×10^{-5}	7.1×10^{-6}	4.2×10^{-6}	2.275646	1.126714	0.071381	1.7×10^{-5}	1.0×10^{-5}	5.9×10^{-6}	0.706	0.710	0.712
2.80	0.60	2.569214	1.225741	0.064214	1.0×10^{-5}	6.2×10^{-6}	3.8×10^{-6}	2.554313	1.220054	0.064382	1.4×10^{-5}	8.8×10^{-6}	5.3×10^{-6}	0.714	0.705	0.717
2.80	0.80	2.841421	1.312214	0.058214	8.9×10^{-6}	5.5×10^{-6}	3.3×10^{-6}	2.823236	1.305495	0.058382	1.3×10^{-5}	7.8×10^{-6}	4.6×10^{-6}	0.685	0.705	0.717
2.80	1.00	3.106241	1.391214	0.052741	7.6×10^{-6}	4.8×10^{-6}	2.9×10^{-6}	3.084497	1.383423	0.052907	1.1×10^{-5}	6.8×10^{-6}	4.1×10^{-6}	0.691	0.706	0.707

Furthermore, the residual errors RE_{ϕ_1}, RE_{ϕ_2}, and RE_{ϕ_3} decrease systematically as σ increases from 0.2 to 1.0. This progressive reduction confirms the stable convergence behavior of the proposed APEIS framework while maintaining high computational accuracy throughout the considered parameter domain. In comparison with ADM, the APEIS produces lower residual errors for the tested cases, which confirms its improved numerical reliability for the considered fractional nonlinear dynamical system.

Figure 1 presents the mean residual errors obtained by the proposed APEIS and the classical ADM for different fractional orders. The blue curve corresponds to the APEIS, whereas the red curve represents the ADM. Lower residual-error values indicate higher numerical accuracy. It can be observed that the residual errors decrease as the fractional order σ increases for both methods. Moreover, the APEIS consistently produces smaller residual errors than the ADM over the entire range of fractional orders, demonstrating its superior numerical accuracy and convergence performance.

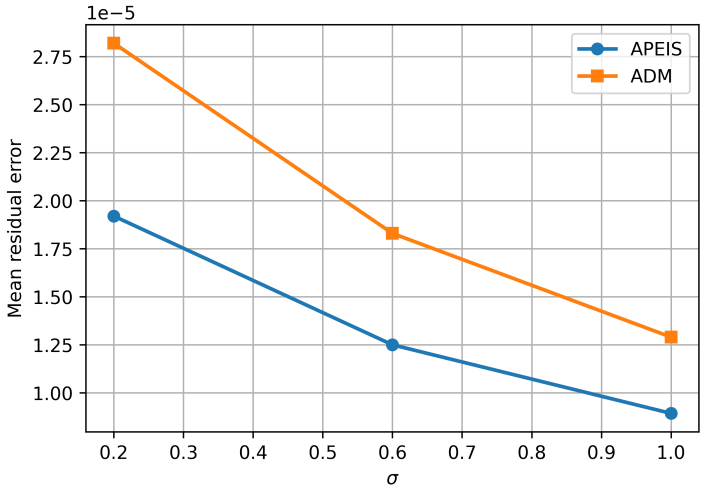


Figure 1. Comparison of the mean residual errors obtained by the APEIS and ADM approximations for different values of σ.

In the following subsections, wave dynamics generated by the TF-HR system are investigated at the fixed temporal level $\mu_2 = 1.00$. The objective is to examine how different fractional orders influence nonlinear oscillatory behavior, propagation characteristics, and memory-dependent dynamical responses.

5.3. Wave dynamics and nonlinear signal behavior

This subsection investigates the wave propagation characteristics generated by the TF-HR system under different fractional orders. Particular attention is devoted to examining how memory-dependent mechanisms influence nonlinear oscillatory behavior, adaptive responses, and propagation dynamics. To provide a clearer interpretation of the generated wave structures, graphical representations are employed to visualize behavior of the state variables under different fractional-memory regimes.

Figure 2 presents the wave profiles of the three state variables, ϕ_1, ϕ_2, and ϕ_3, obtained from system (4.1) at the fixed time level $\mu_2 = 1.00$ with the fractional order $\sigma = 0.2$. The subplots respectively illustrate the spatial evolution of the principal signal, recovery, and adaptation variables. The relatively small fractional order introduces stronger memory effects, resulting in smoother wave propagation and slower dynamical evolution. The principal state variable ϕ_1 exhibits stable nonlinear oscillations, whereas ϕ_2 and ϕ_3 display slower recovery and adaptation dynamics due to the stronger memory influence.

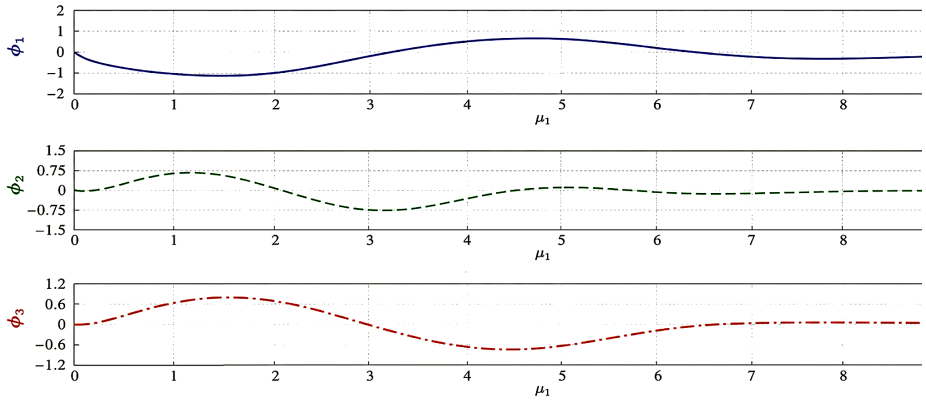


Figure 2. Wave behavior of system (4.1) at $\mu_2 = 1.00$ and $\sigma = 0.2$.

Figure 3 presents the wave profiles of the three state variables, ϕ_1, ϕ_2, and ϕ_3, obtained from system (4.1) at the fixed time level $\mu_2 = 1.00$ with the fractional order $\sigma = 0.6$. The subplots respectively illustrate the spatial evolution of the principal signal, recovery, and adaptation variables. Compared with the case of $\sigma = 0.2$, the wave profiles exhibit more balanced dynamical behavior due to the moderate memory effects. The interaction among nonlinear oscillations, recovery mechanisms, and adaptive responses becomes more pronounced, indicating stronger dynamical interactions while maintaining controlled memory influence.

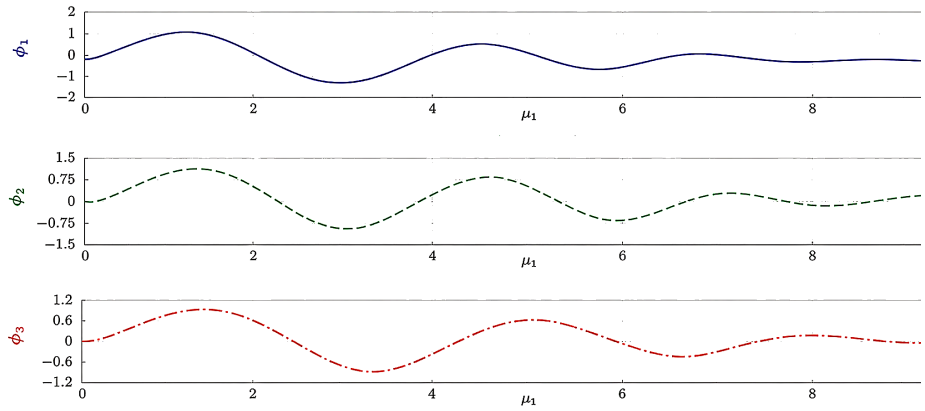


Figure 3. Wave behavior of system (4.1) at $\mu_2 = 1.00$ and $\sigma = 0.6$.

Figure 4 presents the wave profiles of the three state variables, ϕ_1, ϕ_2, and ϕ_3, obtained from system (4.1) at the fixed time level $\mu_2 = 1.00$ with the fractional order $\sigma = 1.00$. The subplots respectively illustrate the spatial evolution of the principal signal, recovery, and adaptation variables. The wave profiles exhibit stronger oscillatory activity together with faster dynamical evolution due to the weaker influence of fractional memory. Consequently, the numerical solution gradually approaches the classical integer-order behavior, showing reduced long-memory effects while preserving the nonlinear interaction among the three state variables.

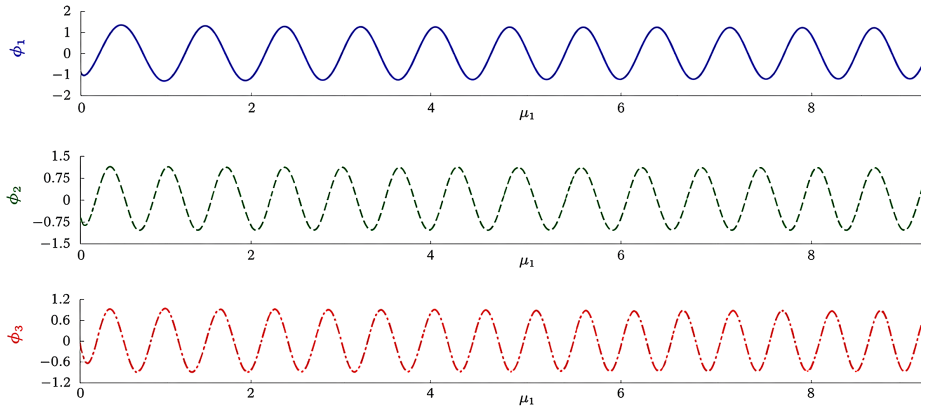


Figure 4. Wave behavior of system (4.1) at $\mu_2 = 1.00$ and $\sigma = 1.00$.

Figure 5 compares the wave dynamics under different fractional orders. The results demonstrate that decreasing fractional order strengthens memory-dependent mechanisms and produces smoother dynamical behavior, whereas increasing fractional order generates stronger oscillatory responses together with faster dynamical evolution. Consequently, the fractional order parameter acts as an effective mechanism influencing oscillatory behavior, memory effects, and adaptive dynamical responses.

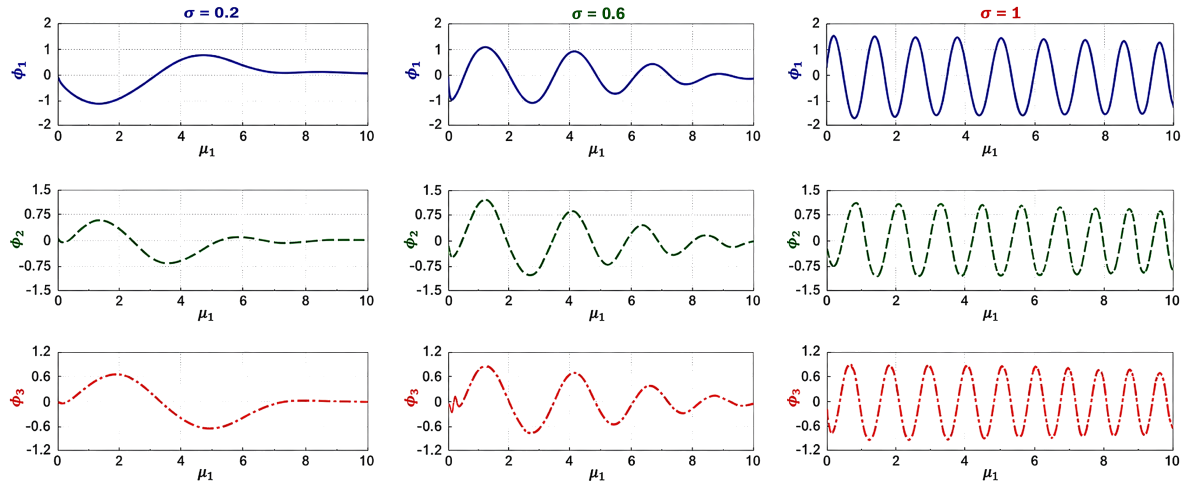


Figure 5. Comparison of wave behavior for (4.1) at $\mu_2 = 1.00$ with $\sigma = 0.20, 0.60, 1.00$.

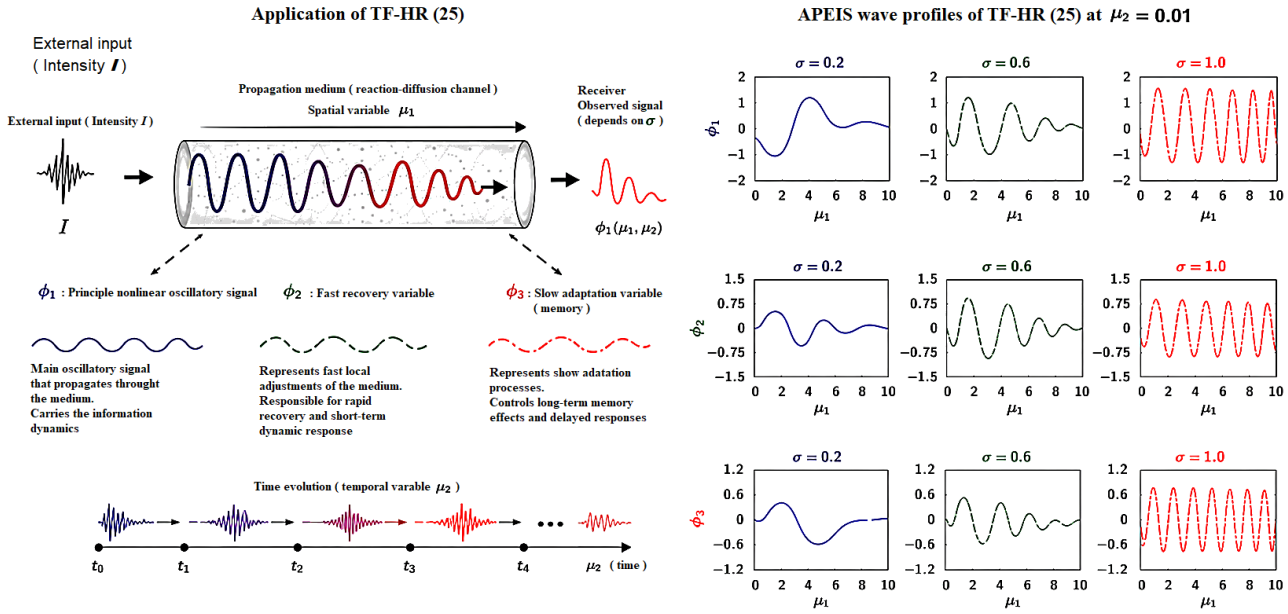


Figure 6. Application of the TF–Hindmarsh–Rose reaction–diffusion system to memory-dependent nonlinear signal propagation.

Figure 6 illustrates the application of the TF–Hindmarsh–Rose reaction–diffusion system to memory-dependent nonlinear signal propagation. The left panel depicts the transmission of an oscillatory information signal through a nonlinear medium, where ϕ_1 represents the principal oscillatory signal, ϕ_2 corresponds to the fast recovery dynamics, and ϕ_3 describes the slow adaptation variable associated with memory effects. The right panel displays the corresponding APEIS wave profiles for several values of the fractional-order parameter σ. It is observed that decreasing σ

strengthens the memory effect, resulting in smoother and more attenuated wave propagation, whereas increasing σ weakens the memory influence and leads to larger-amplitude and more persistent oscillatory behavior.

5.4. Interpretation of nonlinear signal dynamics

The obtained numerical results demonstrate that the TF-HR system provides a flexible mathematical framework to investigate nonlinear signal dynamics and memory-dependent propagation behavior. The nonlinear oscillatory variable ϕ_1 acts as principal oscillatory component, whereas ϕ_2 controls rapid recovery responses associated with fast dynamical adjustments. Meanwhile, ϕ_3 governs slow adaptive responses together with long-memory effects. The generated wave structures indicate that fractional memory play an important role in controlling dynamical behavior and propagation characteristics. Smaller fractional orders generate smoother oscillatory structures with stronger memory influence, whereas larger fractional orders produce faster dynamical evolution together with reduced memory effects. Consequently, the fractional parameter provides an additional mechanism influencing nonlinear dynamics that is unavailable in classical integer-order models.

Furthermore, generated dynamics suggest potential applications to investigate nonlinear signal generation, propagation behavior, adaptive responses, and memory-dependent dynamical processes.

5.5. Discussion and practical implications

This work presented a numerical investigation of the TF-HR system through the proposed APEIS framework. Since the considered nonlinear fractional model does not admit closed-form exact solutions, analysis was performed using approximate solutions, convergence behavior, residual-error evaluation, and wave dynamics investigations. In addition, a comparative study with the classical ADM was conducted to assess the accuracy and reliability of the proposed approach. The numerical results demonstrated that the APEIS framework provides stable, accurate, and reliable approximations with satisfactory convergence characteristics. The residual-error analysis confirmed the effectiveness of the proposed computational procedure, while the comparison with the ADM revealed a close agreement between the two methods and showed that the APEIS consistently produces smaller residual errors, indicating improved numerical accuracy and convergence performance. The generated wave structures revealed that fractional memory plays significant role in shaping nonlinear signal propagation, recovery mechanisms, and adaptive responses. In particular, smaller fractional orders produced smoother dynamical evolution accompanied by stronger memory effects, whereas larger fractional orders generated faster oscillatory behavior with reduced memory influence. These observations indicate that the fractional-order parameter provides an additional degree of flexibility for controlling nonlinear dynamical behavior beyond that available in classical integer-order formulations.

Overall, the obtained results confirm that the TF-HR framework combined with the APEIS methodology constitutes an effective mathematical and computational tool to investigate nonlinear signal dynamics, memory-dependent propagation phenomena, and adaptive dynamical processes in fractional reaction–diffusion systems.

6. Conclusions

In this work, the proposed APEIS framework was successfully developed and applied to investigate the TF-HR system involving ABC fractional operators. Theoretical results concerning existence, uniqueness, convergence, and Hyers–Ulam stability were established, providing a rigorous mathematical foundation for the proposed methodology. The numerical investigations demonstrated that the APEIS generates accurate approximations with satisfactory convergence behavior and consistently small residual errors. Comparisons with the classical ADM confirmed the reliability and effectiveness of the proposed framework. Furthermore, the numerical results showed that fractional memory significantly influences nonlinear oscillatory dynamics. In particular, smaller fractional orders produce smoother dynamical evolution with stronger memory effects, whereas larger fractional orders lead to faster oscillatory behavior with weaker memory influence. The proposed APEIS framework is applicable to a broad class of nonlinear fractional systems involving the ABC operator under the assumptions established in the theoretical analysis. The time-fractional Hindmarsh–Rose system serves as a representative application demonstrating the effectiveness of the proposed methodology. Future work will focus on extending the proposed APEIS framework to a wider class of nonlinear fractional differential systems involving different fractional operators and more complex reaction–diffusion models. In addition, further studies will investigate computational efficiency through detailed comparisons of CPU time, memory requirements, and computational complexity with existing numerical methods. The application of the APEIS to additional benchmark problems and practical engineering and biological models will also be considered to further demonstrate its generality and robustness.

Overall, the obtained results demonstrate that the proposed APEIS framework provides an accurate, reliable, and efficient tool for investigating memory-dependent nonlinear reaction–diffusion systems.

Principal symbols

Symbol	Description
Π_Ψ	Computational domain.
Ψ	Spatial domain.
(μ_i)	Vector of independent variables.
μ_m	Fractional time variable.
ϕ_k	Unknown state variable.
σ	Fractional order ($0 < \sigma \leq 1$).
$\mathcal{D}^{\sigma}_{0,\mu_m}$	Atangana–Baleanu–Caputo fractional derivative.
$\mathcal{I}^{\sigma}_{0,\mu_m}$	Atangana–Baleanu fractional integral.
$\mathcal{Q}_k$	Nonlinear operator.
$\mathcal{F}_k$	Continuous delay function.
ρ_k	Delay bound.
ω_{ϕ_k}	Lipschitz constant.
η	Contraction factor.
H_σ	Hyers–Ulam stability constant.
S^d_k	dth APEIS approximation.
$\phi_{k,n}$	nth APEIS coefficient.
RE_{ϕ_k}	Residual error.
D_{ϕ_k}	Diffusion coefficient.
I	External input parameter.

Author contributions

Othman Abdullah Almatroud: Conceptualization, formal analysis, investigation, project administration, writing–original draft; Faten H. Damag: Conceptualization, investigation, methodology, writing–review and editing; Sahar Albosaily: Methodology, software, writing–review and editing; Marwa Ennaceur: Formal analysis, software, methodology, writing–review and editing. All authors have read and agreed to the published version of the manuscript.

Use of Generative-AI tools declaration

The authors declare they have not used Artificial Intelligence (AI) tools in the creation of this article.

Conflict of interest

The authors declare no conflicts of interest.

Funding

This research has been funded by the Scientific Research Deanship at University of Ha'il-Saudi Arabia through project number RG-25 039.

References

1. A. Iqbal, R. Nawaz, H. Hina, A. G. Ahmad, H. Emadifar, Utilizing the optimal auxiliary function method for the approximation of a nonlinear long wave system considering Caputo fractional order, *Complexity*, **2024** (2024), 8357221. https://doi.org/10.1155/2024/8357221
2. K. Shah, A. R. Seadawy, M. Arfan, Evaluation of one dimensional fuzzy fractional partial differential equations, *Alex. Eng. J.*, **59** (2020), 3347–3353. https://doi.org/10.1016/j.aej.2020.05.003
3. R. Ashraf, R. Nawaz, O. Alabdali, N. F. Young, A. H. Ali, F. Ghanim, et al., A new hybrid optimal auxiliary function method for approximate solutions of nonlinear fractional partial differential equations, *Fractal Fract.*, **7** (2023), 673. https://doi.org/10.3390/fractalfract7090673
4. A. E. Hamza, O. Osman, A. Ali, A. Alsulami, K. Aldwoah, A. Mustafa, et al., Fractal-fractional-order modeling of liver fibrosis disease and its mathematical results with subinterval transitions, *Fractal Fract.*, **8** (2024), 638. https://doi.org/10.3390/fractalfract8110638
5. H. N. Zaidi, O. Osman, A. Dawood, A. Saif, A. S. Awaad, K. Aldwoah, et al., Solvability and stability analysis of three-dimensional ABC fractional systems in locally compact Hausdorff spaces: Applications to chaotic and fluid systems, *Fractal Fract.*, **10** (2026), 214. https://doi.org/10.3390/fractalfract10040214
6. H. N. Zaidi, A. Saif, M. Suhail, N. Haron, A. S. Awaad, K. Aldwoah, et al., A semi-analytical and topological study of fractional dynamical systems in Banach spaces endowed with the compact-open topology: Applications to wave propagation phenomena, *Fractal Fract.*, **10** (2026), 181. https://doi.org/10.3390/fractalfract10030181
7. M. Adel, K. Aldwoah, F. Alahmadi, M. S. Osman, The asymptotic behavior for a binary alloy in energy and material science: The unified method and its applications, *J. Ocean Eng. Sci.*, **9** (2024), 373–378. https://doi.org/10.1016/j.joes.2022.03.006
8. F. H. Damag, A. Saif, M. Alshammari, F. Alhubairah, M. F. Alshammari, M. S. Alsharafi, Hybrid expansion methods for fractional nonlinear mathematical systems with Erdelyi–Kober derivative operators in the theory of tsunami wave modeling, *Sci. Rep.*, **16** (2026), 10551. https://doi.org/10.1038/s41598-026-46268-5
9. Y. Li, F. Liu, I. W. Turner, T. Li, Time-fractional diffusion equation for signal smoothing, *Appl. Math. Comput.*, **326** (2018), 108–116. https://doi.org/10.1016/j.amc.2018.01.007
10. K. A. Aldwoah, M. A. Almalahi, K. Shah, M. Awadalla, R. H. Egami, Dynamics analysis of dengue fever model with harmonic mean type under fractal-fractional derivative, *AIMS Math.*, **9** (2024), 13894–13926. https://doi.org/10.3934/math.2024676

11. F. H. Damag, A. Saif, On solving modified time Caputo fractional Kawahara equations in the framework of Hilbert algebras using the Laplace residual power series method, *Fractal Fract.*, **9** (2025), 301. https://doi.org/10.3390/fractalfract9050301
12. T. Yazgan, E. Ilhan, E. Çelik, H. Bulut, On the new hyperbolic wave solutions to Wu–Zhang system models, *Opt. Quant. Electron.*, **54** (2022), 298. https://doi.org/10.1007/s11082-022-03683-y
13. A. R. Seadawy, M. Iqbal, D. Lu, Propagation of kink and anti-kink wave solitons for the nonlinear damped modified Korteweg–de Vries equation arising in ion-acoustic waves in an unmagnetized collisional dusty plasma, *Physica A*, **544** (2020), 123560. https://doi.org/10.1016/j.physa.2019.123560
14. A. Akgul, A. Cordero, J. R. Torregrosa, A fractional Newton method with 2α-order of convergence and its stability, *Appl. Math. Lett.*, **98** (2019), 344–351. https://doi.org/10.1016/j.aml.2019.06.028
15. B. R. Sontakke, A. S. Shelke, A. S. Shaikh, Solution of nonlinear fractional differential equations by variational iteration method and applications, *Far East J. Math. Sci.*, **1** (2019), 113–129. https://doi.org/10.17654/MS110010113
16. A. Shams, E. Mohamed, A. Abdelgabar, H. Walid, Numerical solutions of time-fractional Whitham–Broer–Kaup equations via Sumudu decomposition method, *J. Math.*, **2023** (2023), 4664866. https://doi.org/10.1155/2023/4664866
17. S. M. El-Sayed, D. Kaya, Exact and numerical traveling wave solutions of Whitham–Broer–Kaup equations, *Appl. Math. Comput.*, **167** (2005), 1339–1349. https://doi.org/10.1016/j.amc.2004.08.012
18. B. Boutarfa, A. Akgul, M. Inc, New approach for the Fornberg–Whitham type equations, *J. Comput. Appl. Math.*, **312** (2017), 13–26. https://doi.org/10.1016/j.cam.2015.09.016
19. H. Xu, W. Cheng, J. Cui, Multiple-soliton and periodic solutions to space-time fractional Whitham–Broer–Kaup equations, *Eur. Phys. J.-Spec. Top.*, **231** (2022), 2353–2357. https://doi.org/10.1140/epjs/s11734-021-00374-9
20. R. Shah, H. Khan, D. Baleanu, Fractional Whitham–Broer–Kaup equations within modified analytical approaches, *Axioms*, **8** (2019), 125. https://doi.org/10.3390/axioms8040125
21. O. Nikan, J. Rashidinia, H. Jafari, An improved local radial basis function method for pricing options under the time-fractional Black–Scholes model, *J. Comput. Sci.*, **89** (2025), 102610. https://doi.org/10.1016/j.jocs.2025.102610
22. W. Li, W. Bai, J. Cao, Turing instability and pattern formation in a diffusive predator–prey system with opportunistic predators and weak Allee effect, *Phys. Rev. E*, **113** (2026), 044219. https://doi.org/10.1103/5fx7-q41y
23. I. S. Fateev, A. A. Polezhaev, Dynamics of a chain of interacting neurons with nonlocal coupling given by Laplace operator of fractional and variable orders with nonlinear Hindmarsh–Rose model functions, *B. Lebedev Phys. Inst.*, **50** (2023), 243–252. https://doi.org/10.3103/S1068335623060039
24. R. Xue, X. Fu, Random attractors for fractional stochastic Hindmarsh–Rose equations with memristors, *J. Dyn. Control Syst.*, **31** (2025), 36. https://doi.org/10.1007/s10883-025-09758-9

25. K. A. Abro, I. Q. Memon, K. S. Mohamed, K. Aldwoah, Neurobiological transition of magnetized and demagnetized dynamism for fractional Hindmarsh–Rose neuron model via fractal numerical simulations, *J. Comput. Electron.*, **24** (2025), 33. https://doi.org/10.1007/s10825-024-02243-9

26. S. A. Malik, A. H. Mir, Discrete multiplierless implementation of fractional order Hindmarsh–Rose model, *IEEE TETCI*, **5** (2020), 792–802. https://doi.org/10.1109/TETCI.2020.2979462

27. M. Xiao, *Stability analysis and Hopf-type bifurcation of a fractional order Hindmarsh–Rose neuronal model*, In: J. Wang, G. G. Yen, M. M. Polycarpou, Eds., Advances in Neural Networks–ISNN 2012, Lecture Notes in Computer Science, Berlin, Heidelberg: Springer, **7367** (2012), 202–209. https://doi.org/10.1007/978-3-642-31346-2_25

28. F. H. Damag, A. Kiliçman, M. Amin, Topological analysis with some techniques for solving a fractional tsunami shallow water mathematical model based on Hausdorff locally compact structures and their analytical implications, *AIMS Math.*, **11** (2026), 3957–3985. https://doi.org/10.3934/math.2026159

29. W. Alfwzan, S. W. Yao, F. M. Allehiany, S. Ahmad, S. Saifullah, M. Inc, Analysis of fractional nonlinear tsunami shallow-water mathematical model with singular and non-singular kernels, *Results Phys.*, **52** (2023), 106707. https://doi.org/10.1016/j.rinp.2023.106707

30. I. A. Rus, Ulam stabilities of ordinary differential equations in a Banach space, *Carpathian J. Math.*, **26** (2010), 103–107.



AIMS Press

© 2026 the Author(s), licensee AIMS Press. This is an open access article distributed under the terms of the Creative Commons Attribution License (https://creativecommons.org/licenses/by/4.0)